Ocean Engineering 153 (2018) 154–172

Contents lists available at ScienceDirect

Ocean Engineering

journal homepage: www.elsevier.com/locate/oceaneng

# Estimating on-site wave spectra from the motions of a semi-submersible platform: An assessment based on model scale results

J. Mas-Soler [a,*], Alexandre N. Simos [a], Eduardo A. Tannuri [b]

[a] Naval Arch. & Ocean Eng. Department, Escola Politécnica. University of São Paulo (USP), Brazil
[b] Mechatronics Eng. Department, Escola Politécnica. University of São Paulo (USP), Brazil

ARTICLE INFO

*Keywords:*
Semi-submersible platform
Damping estimation
Bayesian modelling
Directional wave spectra
Severe sea states

ABSTRACT

This article presents the results of a preliminary investigation on the use of the motions of a large-volume semi-submersible platform as the basis for estimating waves on-site. The main focus of the application is on the harsher wave conditions, for which other measurement devices are known to present limitations. As a first step in this investigation, a series of tests were performed with a scaled model in a wave basin. A wide range of waves was tested in order to evaluate how the estimation errors behave with respect to wave period and amplitude. Moreover, since the statistical inference relies on a linear dynamic model, the influence of uncertainties on the unit's RAOs must be assessed. Since the non-linear viscous effect on resonant responses is known to be one of the main sources of error in this regard, different approaches for predefining the viscous damping levels are tested and compared. The results attest that, at least in the controlled conditions of the tests, the inference method is able to provide accurate estimations of the extreme waves conditions that were tested. A simple method for predicting the damping based on the recorded motions is shown to improve the estimations.

## 1. Introduction

Directional wave inference obtained from the records of vessels motions is a technique that has seen its application grow significantly over the last years. Usually, the main interest in this approach comes from the fact that this sort of estimation only requires simple instrumentation and hardware, which can be easily installed on-board and require little maintenance. Most of the previous works on the method based their estimations on ships or ship-shaped platforms, due to the fact that these vessels are known to have significant response even for mild wave conditions.

The major shortcoming of the method is that only waves that impose a reasonable level of motions to the vessel may be inferred. This is due to the fact that the vessel usually acts as a low-pass filter, filtering the high frequency components that do not excite the vessels first-order responses. Therefore, the larger the vessel, or the lower its response in waves, the more restricted will be the estimation range. The main motivation for this paper, however, arises from the fact that, although a semi-submersible is designed for responding only weakly to the incoming waves, it will still present significant motions in more severe wave conditions and, in these situations, it may perhaps provide a reliable account on the sea state that imposed such motions. For this reason, this method of wave inference is not intended for providing broad oceanographic records, but rather to be used as a means for identifying wave conditions that impose considerable motions on the vessel in which the system is based on.

Another practical reason that motivates the adoption of a large semi-submersible platform as a motion-based wave sensor is that the measuring systems that are widely considered as a global standard for wave data, such as wave buoys (Gemmrich et al., 2016) and wave radar systems (Fucile et al., 2016), may present some drawbacks in extreme weather conditions. For instance, wave buoys may be dragged through or swerve around the 3D peaks of waves (Allender et al., 1989). In addition, eventual presence of a spike in the raw accelerometer data ( Mackay, 2009) may produce erratic maximum wave height measurements. Rough sea states and adverse weather conditions are also among the possible sources of errors in wave measurements from wave radar systems, since errors can be attributed to the shadowing effects produced by rain, large waves or sea spray, as well as the inherent bias of the system that could be increased by extreme sea conditions (Magnusson, 2008). Furthermore, all of them require important initial investments and/or high maintenance costs.

Consequences of these shortcomings are either way important for marine operations, engineering design and validation of forecasts of extreme wave events. In addition, comparisons between estimations

* Corresponding author.
*E-mail address:* jordi@tpn.usp.br (J. Mas-Soler).

https://doi.org/10.1016/j.oceaneng.2018.01.069
Received 16 March 2017; Received in revised form 12 January 2018; Accepted 15 January 2018

obtained with wave buoys and wave radars have shown some important discrepancies (Durrant et al., 2009; Chen et al., 2013; Wijaya, 2009), highlighting the inherent biasses and differences in the performance of the sensors.

For the reasons exposed above, if proven feasible for real conditions, wave estimations obtained from the motions of a semi-submersible platform may provide an interesting complement to the readings of other devices in harsh seas. In fact, they are not expected to be affected by some of the factors mentioned above. On the other hand, it may have to deal with other problems, as for example the non-linear behavior of the motions (especially due to viscous damping effects) induced by the flow on the hull, risers and mooring lines. These aspects will be discussed with detail in this article.

From a general point of view, there are several approaches that may be considered for performing the wave inference based on the recorded motions of a vessel. As a first option, the wave spectrum can be estimated with a parametric modelling, with some examples of this method provided by: Hua and Palmquist (1994), where the wave conditions are estimated using the full-scale data, applying a variational method. Another work based in this research topic is presented by Tannuri et al. (2003), who used the data from a moored FPSO with a non-linear parametric model to estimate the directional wave spectrum. Montazeri and Nielsen (2014) use the parametric approach to estimate the directional wave spectrum from full-scale response measurements carried out on a container ship. One additional example of the parametric modelling approach can be found in Montazeri et al. (2015), which presents a trend analysis for prediction of sea state parameters using a JONSWAP model. Finally, Montazeri et al. (2016) is another recent work in which a parametric model of the directional wave spectrum is calibrated to estimate wind sea and swell based on motions of a ship.

Alternatively, another line of works proposes the estimation of the directional wave spectrum based on non-parametric modelling methods. The inference is then made using either the wave buoy analogy or the Bayesian modelling procedure. Regarding the wave buoy analogy, Nielsen and Stredulinsky (2012) obtain the estimations from full-scale motions measurements. The results are compared with real wave rider buoys and radar data. They show that the statistical parameters are accurately estimated when compared with the wave rider buoy, and the method provides a slightly better estimation when compared to the wave radar systems. Furthermore, Nielsen et al. (2016) aim to evaluate a novel concept for wave estimation using the wave buoy analogy using shipboard measurements, which in this case is formulated directly in the time domain combining different techniques and the least squares fitting to estimate wave amplitude and phase.

The so-called Bayesian modelling procedure has been adopted by Nielsen (2006), who presented derivations of both parametric and non-parametric theories. The theories for both methods are applied in order to obtain the directional wave spectrum from real scale data (radar) and numerical simulations. The same researcher (Nielsen, 2007) carried out a detailed study of numerical simulations of time histories, providing an estimation of the sea state parameters. In this work, two approaches are considered: the parametric procedure and the non-parametric one. The paper finally concludes that it is difficult to favor one particular method, since both of them provide similar results.

Simos et al. (2010) present a complete analysis of the sea states estimated from the motions of a model scale FPSO. These estimations are performed using the Bayesian inference method with two hyperparameters, as proposed by Nielsen (2008), but with a relevant conceptual change. Different from the original proposal, they have set a pre-calibration of these hyperparameters, meaning that the values of both were prescribed for each wave estimation. From a conceptual point of view, although the mathematical structure of the Bayesian model was preserved, an important feature of the Bayesian approach was abandoned, namely the adoption of an information criterion for searching the best values of the hyperparameters in each estimation event. This approach, however, led to a much more expedite estimation procedure, meanwhile the results obtained in the experimental campaign attested that the wave conditions could still be inferred with good accuracy.

Later, Simos et al. (2012) used full-scale data from an FPSO operating in Brazil's Campos basin for a first evaluation of the performance of this method in field conditions. However, due to the lack of alternative wave sensors, the comparison of the results was made almost exclusively with hindcast predictions provided by NOAA for the same region where the FPSO was operating. The authors concluded that the method was capable of inferring the sea states with a good agreement with the NOAA predictions, despite the inherent limitations concerning the estimation of sea states with low peak periods.

Bispo et al. (2016) presents the first part of the results from a new field campaign, started in December 2014. Again, results are obtained from full-scale FPSO motions using the Bayesian inference approach. The performance of the motion-based method is checked against the wave estimations provided by a commercial marine radar system. Comparisons between both systems attest an adequate identification of mean wave conditions.

The use of a semi-submersible platform to estimate extreme wave conditions was initially investigated by Wijaya (2009). As for the present paper, their work was also based in large part on model-scale tests. However, the analysis was based on a set of final design tests performed for the platform, which only comprised a short range of wave conditions.

In the present study, a scaled model of the same semi-submersible unit was built and tested in a large set of experimental conditions at the CH-TPN wave basin of the University of São Paulo. The experiments were specifically conceived for verifying the feasibility of performing the motion-based estimations, putting special emphasis on more severe wave conditions.

Next, a brief description of the statistical inference approach is presented (section 2), followed by the presentation of the semi-submersible unit adopted as a case study (section 3). Section 4 discusses the numerical modelling leading to the linear motion RAOs. It also addresses the importance of a proper damping estimation for predicting the heave resonant motions and the difficulties imposed by the non-linear character of the viscous effects. The experimental setup and the main features of the test campaign are presented in section 5. Section 6 brings the main results, confronting the directional wave spectra estimated by the model motions to those obtained from a set of conventional wave probes. Finally, section 7 draws the main conclusions and discusses further steps that should be taken in the continuity of the research.

## 2. Bayesian inference method

The non-parametric approach adopted in this study follows the Bayesian modelling procedure as proposed by Akaike (1980), which essentially aims at introducing different kinds of *a-priori* information to improve the ill-conditioned problem as well as to reduce the influence of noise. This central idea was used for the first time by Iseki and Ohtsu (2000) to estimate the wave spectrum from measured motions of a ship with forward speed. In their approach, the prior information essentially concerns the fact that the spreading of wave energy in direction should happen smoothly. The trade-off between the good fit to the data and the smoothness of the solution is then controlled through a single hyperparameter. Following these works, Nielsen (2008) proposed the introduction of an additional hyperparameter, which, in its turn, controls the smoothness of the energy distribution regarding the wave frequency. Common to all these previous applications of motion-based wave inference is the fact that the determination of the optimal value of the hyperparameters have been done by minimizing Akaike's Bayesian Information Criterion (ABIC), see e.g. Akaike (1980), despite the expensive computational cost that is required by this procedure.

Simos et al. (2012) and Bispo et al. (2016) used an approach similar to the one proposed by Nielsen (2008). In their case, however, applications were made for moored floating systems (therefore without advance speed) and a third hyperparameter was included, which avoids excessive

energy estimation at frequency boundaries. Apart from these differences, the main modification proposed concerned the estimation of the hyper-paramters, which in the case of Simos et al. (2012) and Bispo et al. (2016) are defined prior to the estimations, following the procedure proposed by Bispo et al. (2012).

The method adopted in the present article follows closely the one proposed in Simos et al. (2012) for moored floating units. For this reason, only a short introduction to the method will be presented next. For the reader who is interested in a more detailed description of the statistical inference approach, it is important to mention that a concise derivation of the formulae concerning the Bayesian method can also be found in Nielsen (2008).

Assuming that the relation between the waves and the ship response is linear, the directional wave spectrum ($S(\omega,\theta)$) and the RAOs (Response Amplitude Operators) are related to the cross spectra derived from the ship motions records ($\phi_{ij}$) through the integral:

$$\phi_{ij}(\omega) = \int_{-\pi}^{\pi} \mathrm{RAO}_i(\omega,\theta)\mathrm{RAO}_j^*(\omega,\theta)S(\omega,\theta)\mathrm{d}\theta. \tag{1}$$

where $\mathrm{RAO}_i(\omega,\theta)$ corresponds to the Response Amplitude Operator of the motion $i$ at frequency $\omega$ and direction of incidence $\theta$. The relation presented by equation (1) can be rewritten in discrete form assuming the integrand to be constant in each slice, $\Delta\theta = \frac{2\pi}{K}$, leading to:

$$\phi_{ij}(\omega) = \Delta\theta \sum_{k=1}^{K} \mathrm{RAO}_i(\omega,\theta_k)\mathrm{RAO}_j^*(\omega,\theta_k)S(\omega,\theta_k), \tag{2}$$

where $\theta_k = -\pi + (k-1)\Delta\theta$.

If a certain range of $M$ wave frequencies is specified previously, being $\Delta\omega = \frac{\omega_M - \omega_1}{M-1}$, equation (2) can be expressed in a matrix form as follows:

$$B = A\cdot\mathbf{x} + U, \tag{3}$$

Here, the vector B contains a total of $(N^2 \times M)$ elements, which are related to the spectrum and the cross-spectrum, and can be expressed as:

$$B = \begin{bmatrix} b_1 \\ b_2 \\ \vdots \\ b_M \end{bmatrix}, \text{ with } b_m = \begin{bmatrix} \phi_{ii}(\omega_m) \\ \vdots \\ \mathrm{Re}[\phi_{ij}(\omega_m)] \\ \vdots \\ \mathrm{Im}[\phi_{ij}(\omega_m)] \\ \vdots \end{bmatrix}. \tag{4}$$

The RAO matrix is represented by the matrix A, which has $(N^2\cdot M) \times (K\cdot M)$ elements.

$$A = \begin{bmatrix} A_1 & 0 & 0 & \cdots & 0 & 0 \\ 0 & A_2 & 0 & \cdots & 0 & 0 \\ 0 & 0 & \ddots & \cdots & 0 & 0 \\ 0 & 0 & 0 & A_m & 0 & 0 \\ 0 & 0 & 0 & 0 & \ddots & \vdots \\ 0 & 0 & 0 & 0 & \cdots & A_M \end{bmatrix}, \tag{5}$$

where the 0 represents the $(N^2 \times K)$ matrix with null elements. The other matrices represented in A are given by:

$$A_m = \begin{bmatrix} \left|\mathrm{RAO}_i(\omega_m,\theta_1)\right|^2 & \cdots & \left|\mathrm{RAO}_i(\omega_m,\theta_k)\right|^2 & \cdots & \left|\mathrm{RAO}_i(\omega_m,\theta_K)\right|^2 \\ \vdots & & \vdots & & \vdots \\ \mathrm{Re}[\mathrm{RAO}_i(\omega_m,\theta_1)\mathrm{RAO}_j^*(\omega_m,\theta_1)] & \cdots & \mathrm{Re}[\mathrm{RAO}_i(\omega_m,\theta_k)\mathrm{RAO}_j^*(\omega_m,\theta_k)] & \cdots & \mathrm{Re}[\mathrm{RAO}_i(\omega_m,\theta_K)\mathrm{RAO}_j^*(\omega_m,\theta_K)] \\ \vdots & & \vdots & & \vdots \\ \mathrm{Im}[\mathrm{RAO}_i(\omega_m,\theta_1)\mathrm{RAO}_j^*(\omega_m,\theta_1)] & \cdots & \mathrm{Im}[\mathrm{RAO}_i(\omega_m,\theta_k)\mathrm{RAO}_j^*(\omega_m,\theta_k)] & \cdots & \mathrm{Im}[\mathrm{RAO}_i(\omega_m,\theta_K)\mathrm{RAO}_j^*(\omega_m,\theta_K)] \\ \vdots & & \vdots & & \vdots \end{bmatrix}, \tag{6}$$

The vector $\mathbf{x}$ of equation (3) represents the unknown wave spectrum evaluated at the $(K \times M)$ pairs of frequencies and directions:

$$\mathbf{x} = \begin{bmatrix} S(\omega_1,\theta_1) \\ S(\omega_1,\theta_2) \\ \vdots \\ S(\omega_M,\theta_{K-1}) \\ S(\omega_M,\theta_K) \end{bmatrix}. \tag{7}$$

Finally, $U$ is a vector with $(N^2 \times M)$ elements representing the measurement noise, which is assumed to be Gaussian with zero mean value and variance $\sigma^2$.

As suggested by Akaike (1980), the Bayes procedure can be applied in the singular system presented by equation (3). With such procedure, the estimation of the vector $\mathbf{x}$ is obtained maximizing the product of the likelihood function $L(\mathbf{x}|B)$ by the prior distribution, where the likelihood function represents the probability of occurrence of the spectrum given a specific measurement $B$.

As pointed out above, the measurement noise is assumed Gaussian with zero mean and variance $\sigma^2$. Therefore (see Akaike (1980)), the likelihood function is given by:

$$L(\mathbf{x}|B) = \left(\frac{1}{2\pi\sigma^2}\right)^{\frac{N^2}{2}} \exp\left(-\frac{1}{2\sigma^2}\left\|B - A\mathbf{x}\right\|^2\right). \tag{8}$$

The prior distribution $p(\mathbf{x})$ brings information about the unknown coefficients. In this case, the information known *a-priori* relates to the assumption that the wave spectrum is smooth both in direction and frequency. For implementing this, the method makes use of the second order differences $\varepsilon_{1mk}$ and $\varepsilon_{2mk}$, which are associated to the direction $k$ and frequency $m$, and can be simply defined as:

$$\begin{aligned} \varepsilon_{1mk} &= S(\omega_m,\theta_{k-1}) - 2S(\omega_m,\theta_k) + S(\omega_m,\theta_{k+1}), \\ \varepsilon_{2mk} &= S(\omega_{m-1},\theta_k) - 2S(\omega_m,\theta_k) + S(\omega_{m+1},\theta_k). \end{aligned} \tag{9}$$

The smoothness condition is equivalent to keeping the following relations as small as possible:

$$\begin{aligned} \sum_{k=1}^{K}\sum_{m=1}^{M} \varepsilon_{1mk} &= \mathbf{x}^T H_1 \mathbf{x}, \\ \sum_{k=1}^{K}\sum_{m=1}^{M} \varepsilon_{2mk} &= \mathbf{x}^T H_2 \mathbf{x}. \end{aligned} \tag{10}$$

where $S(\omega_m,\theta_0) = S(\omega_m,\theta_K)$.

The matrices $H_1$ and $H_2$ can be easily computed considering the definition of the vector $\mathbf{x}$ (for more information see Nielsen (2008)).

Finally, one must take care of another practical problem: In frequencies for which part or all the motions of the vessel are null, any estimation is possible, and therefore invalid. Thus, in order to avoid an over prediction of the spectrum energy or inconsistent results (due to the null or very small response of the platform), the total energy of the spectrum is minimized in a pre-defined range of low and high frequencies. A third hyperparameter (Simos et al., 2012) is then introduced in order to control the influence of this request in the final solution.

$$\sum_{k=1}^{K}\sum_{m=1}^{L} S(\omega_m,\theta_k)^2 + \sum_{k=1}^{K}\sum_{m=H}^{M} S(\omega_m,\theta_k)^2 = \mathbf{x}^T H_3 \mathbf{x} \tag{11}$$

Considering that each one is a Gaussian variable, with zero mean and variances $(\sigma_1/u_1)^2$, $(\sigma_2/u_2)^2$ and $(\sigma_3/u_3)^2$ for the distributions presented in equations (10) and (11); the product of the likelihood function (see equation (8)) by the prior distribution $p(\mathbf{x})$ is given by:

$$L(\mathbf{x}|B)\cdot p(\mathbf{x}) = C\cdot\exp\left(-\frac{1}{2\sigma^2}\left[||B-A\mathbf{x}||^2 + \mathbf{x}^T\left(u_1^2H_1 + u_2^2H_2 + u_3^2H_3\right)\mathbf{x}\right]\right), \tag{12}$$

where C represents a factor that is independent of the unknown in the model ($\mathbf{x}$). The hyperparameters $u_1$ and $u_2$ control the compromise between a good fit to the data and the smoothness of the estimated spectrum in direction and frequency, respectively. These hyperparameters should be properly calibrated; some works that have been presented in the literature deal with the estimation of the optimal hyperparameters for a specific type of ship -VLCC- (see e.g. Bispo et al. (2012)). In this case, an extensive sensitivity analysis has been performed in order to obtain the optimal values of the hyperparameters. Which are equal to: $u_1$ remains equal as the one presented by Bispo et al. (2012), for $u_2$ the optimal value is given by $1\cdot10^{-5}$ and $u_3$ is equal to 0.0035. The almost negligible value of $u_2$ arises from the narrow differences between the beam and length of the platform, which produce similar RAOs for roll and pitch motions. This resemblance maintains the information level provided by these motions always equilibrated avoiding inconsistent results and therefore larger values of $u_2$ are no longer needed.

Finally, it should be noticed that the total size of the maximization problem is defined by the number of directions (K) and frequencies (M) considered, being the number of variables equal to $K \times M$. From equation (12) this problem can be interpreted as the minimization of the following functional:

$$J(\mathbf{x}) = ||B-A\mathbf{x}||^2 + \mathbf{x}^T\left(u_1^2H_1 + u_2^2H_2 + u_3^2H_3\right)\mathbf{x}. \tag{13}$$

Which is feasible by means of a conventional quadratic programming algorithm.

## 3. Case study

The model employed during the experimental campaign at the CHTPN was a precise scale (1:120) model of the Åsgard-B large semi-submersible processing platform (see Fig. 1). The main dimensions of the platform are given in Table 1, also a 3D sketch and a photo of the model are presented in Fig. 2. The structure of the semi-submersible platform model is mainly composed by a rectangular ring pontoon connected to the deck by six box-shaped columns (4 corner columns and 2 center columns).

**Fig. 1.** Åsgard-B floating gas production platform, from Statoil (2014).

**Table 1**
General geometric properties in full-scale and model-scale.

| Properties | Full-scale | Small-scale |
|---|---|---|
| LOA (m) | 102.4 | 0.853 |
| B (m) | 96.0 | 0.800 |
| D (m) | 45.0 | 0.375 |
| Draft (m) | 25.0 | 0.208 |
| Width of pontoons (m) | 19.20 | 0.16 |
| Height of pontoons (m) | 8.96 | 0.074 |
| Diameter, corner columns (m) | 19.20 | 0.16 |
| Diameter, center columns (m) | 12.20 | 0.10 |
| Displacement (kg) | $8.27\cdot10^7$ | 46.621 |
| Pitch inertia moment (kg· m$^2$) | $1.56\cdot10^{11}$ | 2.25 |
| Roll inertia moment (kg· m$^2$) | $1.21\cdot10^{11}$ | 2.23 |
| Heave natural period (s) | 24 | 2.19 |
| Pitch natural period (s) | 88 | 8.03 |
| Roll natural period (s) | 74 | 6.75 |
| GM Roll (m) | 3.312 | 0.027 |
| GM Pitch (m) | 3.321 | 0.027 |
| KB Roll (m) | 8.362 | 0.069 |
| KB Pitch (m) | 8.362 | 0.069 |
| BM Roll (m) | 26.855 | 0.223 |
| BM Pitch (m) | 27.063 | 0.225 |
| KG Roll (m) | 31.905 | 0.265 |
| KG Pitch (m) | 32.104 | 0.267 |

Wave inference will be made based on the three most significant motions, namely heave, roll and pitch. For this reason, an analysis of the dynamic characteristics of these motions is important. The hydrodynamic properties of the semi-submersible unit are documented in Wijaya (2009) with a heave natural period equal to 24s. The natural periods for the roll and pitch motions are both above the wave frequency range, being defined as 74s and 88s, respectively.

Since it is known that the estimation of a linearized viscous damping is an important source of errors concerning the prediction of the resonant responses, one may realize that this platform indeed has good response characteristics for being used as a wave sensor. In fact, the very large natural periods in roll and pitch are well above the periods of the sea waves, thus increasing the reliability of the RAOs of angular motions within the wave frequency range. Nonetheless, damping corrections in heave motion are still necessary, for this motion presents its resonance inside the range of interest of the current study (focused on large period waves). These corrections were evaluated considering two different approaches: a constant external damping equivalent to 5% of the critical damping (determined experimentally) and a linear damping estimated as a function of the heave amplitude. Further details about the damping corrections will be presented in sections 4 and 5, together with results obtained from decay tests.

### 3.1. Scaled model

The manufacturing process for the model construction took into account the geometrical complexity of the hull and the need to keep the model mass low (in order to guarantee a proper margin for ballast calibration). Considering these restraints, the 3D printing with nylon sintered material was selected as the best method of construction, except for the deck, which was made of Medium Density Fiberboard (top sides were not modeled, as the tests did not include wind effects). The main features of the real scale semi-submersible platform and the model are given in Table 1. The mass properties of the model (no ballast) were confirmed experimentally through two bifilar pendulum test (roll and pitch). Inclination tests in the water were made in order to verify the metacentric heights.

The model was moored to the tank by means of a soft spring horizontal system (above the waterline). The objective of the mooring was only to keep the model offsets within the range of optical motion-tracking system. The stiffness of the system was kept as low as possible, in order to

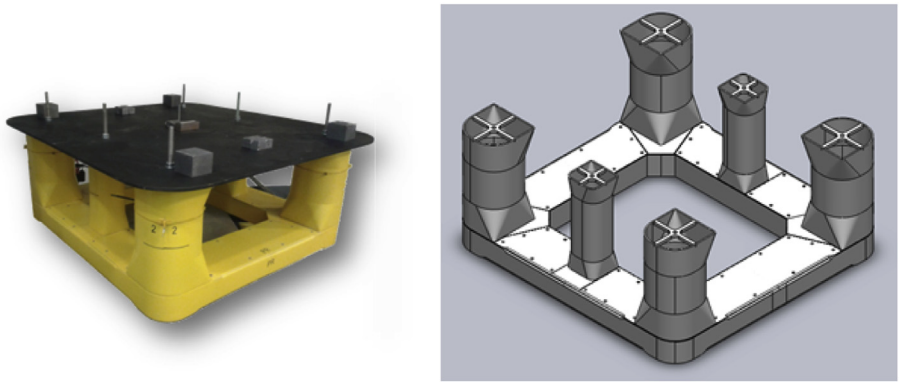

**Fig. 2.** The 1:120 scaled semi-submersible platform model.

have little effect on the first order motions. The overall stiffness in both horizontal directions was confirmed by means of pull-out tests.

## 4. Numerical modelling: motion RAOs and external damping

The motion-based wave estimation is strongly dependent on the accuracy of the RAOs, which characterize the dynamic behavior of the semi-submersible platform. In the present study, the hydrodynamical properties have been obtained with two different approaches: frequency and time-domain analyses. The former was performed to obtain the set of motion RAOs that were used in the wave inference process. On the other hand, time domain simulations were also made in order to support the analysis of the non-linear drag effects, especially those associated with large amplitudes of heave motions near resonance. This section provides a general description of the procedures followed during the numerical modelling, including the analysis of the main results.

### 4.1. Frequency-domain: first-order RAOs

RAOs were computed in frequency-domain using the software WAMIT. The numerical model was made using the higher-order method, which allows the approximation of the geometry by B-splines functions. In our case, the hull geometry was represented by 52 different patches. In this approach, the velocity potential and the fluid velocity on the body are described in a continuous manner inside each patch. Fig. 3 shows the geometry considered in this numerical model.

Fig. 4 shows the RAOs computed in frequency-domain for the heave, roll and pitch motions. Results are presented for five different wave directions, from 180deg. (bow seas) to 90deg. waves (one should remind that the hull is symmetric in both x and y directions). For the sake of illustration, RAOs were computed with external damping equal to 0% and 5% (dashed black line), which is a typical value for the external damping and therefore provides a useful reference. Please notice that the RAOs with 5% of external damping are only provided for the most unfavorable direction regarding each motion, i.e.: 180deg. for heave and pitch and 90deg. for roll motion.

The RAOs reflect the dynamic characteristics of the platform that were emphasized before: the heave motion is the only one with resonance inside the wave-frequency range (therefore, the external damping effect is only significant for the heave RAO); roll and pitch have natural periods around 74 and 88 s, respectively, and therefore their motions within the frequency range are not supposed to be strongly affected by viscous effects.

### 4.2. Time-domain analysis: viscous-effects

As explained before, the aim of the time-domain analysis is to evaluate the viscous drag forces acting on the pontoons of the platform and its impact on the motions, especially when large amplitudes are involved. The impact of the viscous forces on motion RAOs is widely documented in the literature (see for example Clauss et al. (1992)). In the present case, as mentioned above, the major influence of the drag forces should be found in the heave motion. A proper evaluation of these effects is necessary, especially because heave is the most determinant motion for the estimation of wave amplitudes.

The software used during this stage was the ANSYS-AQWA Hydrodynamic Time Response package. In order to perform the analysis in AQWA, 11 830 panels were used in the model. In addition, some parts of the pontoons were modeled as Morison elements in order to introduce the quadratic drag effects.

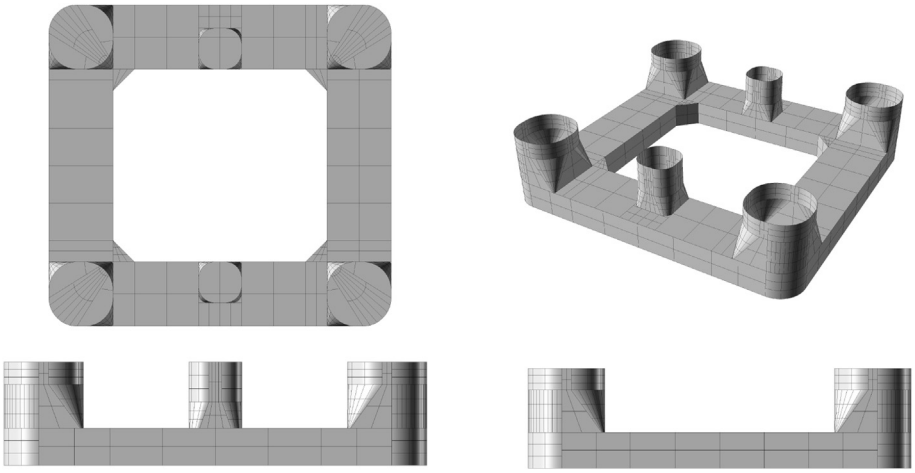

**Fig. 3.** Higher order mesh of the semi-submersible platform.

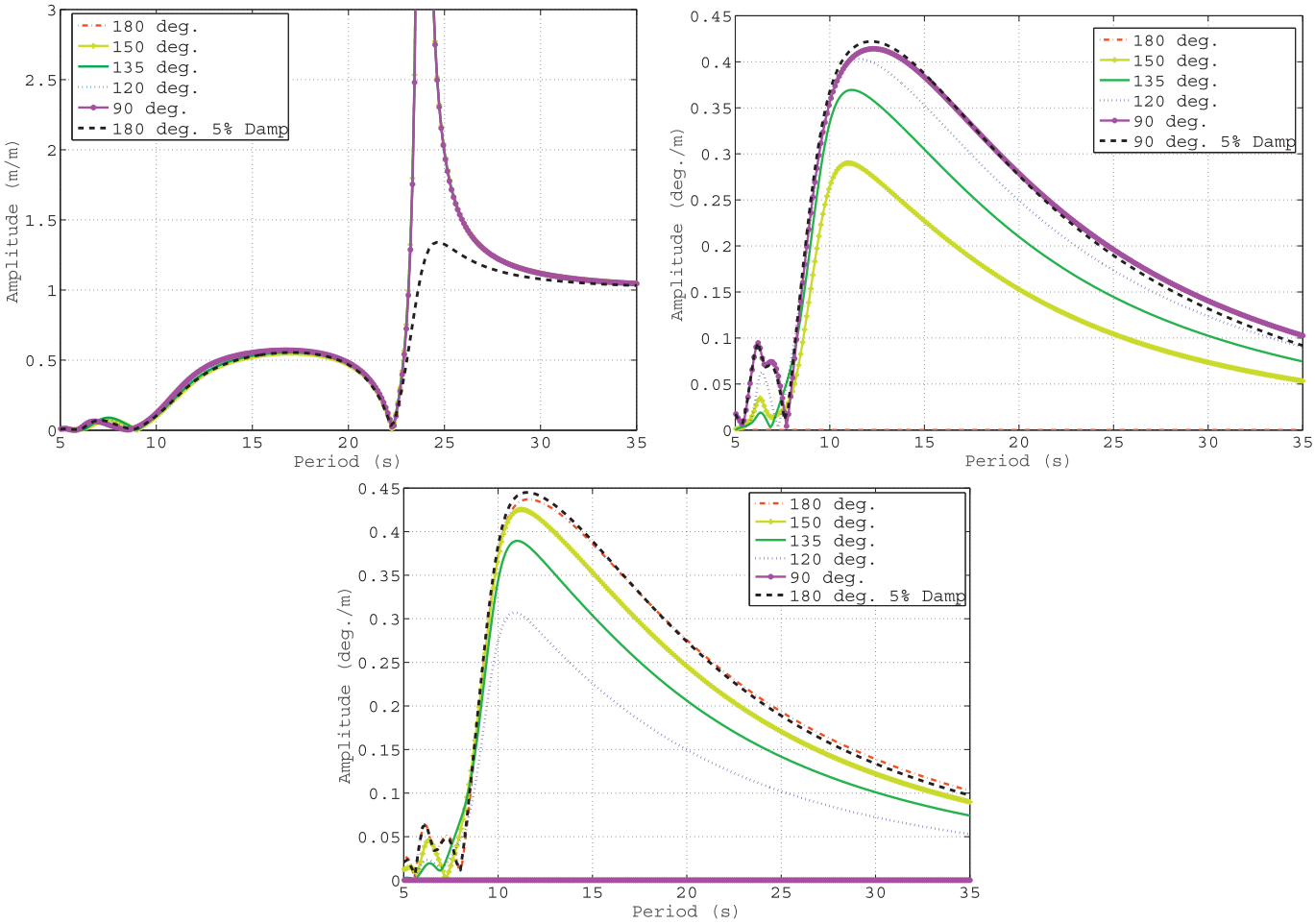


**Fig. 4.** RAOs for the motions of heave, roll and pitch.

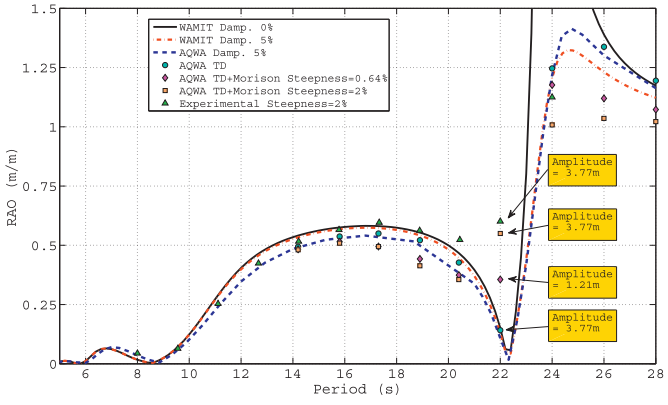


**Fig. 5.** RAO Heave, for the heading of $\beta = 180^{\circ}$.

Fig. 5 provides an illustration of the heave RAO. Only the heading equal to 180° is evaluated here, because the heave responses for the other angles of incidence show only narrow differences if compared to this direction (see Fig. 4). The WAMIT frequency-domain analysis (with 0% and 5% of fixed external damping) provides a basis of comparison for the time-domain study. It can be seen that both codes provide similar results for the computations in frequency-domain with 5% fixed external damping.

The figure also presents the results obtained for different regular wave amplitudes using the AQWA time-domain package (indicated by AQWA TD). A first set of results was obtained for a wave steepness of 2%, without considering the Morison elements on the pontoons (blue circles). It can be seen that the RAO results obtained this way agree quite well with the results obtained from frequency-domain. A second set of results was generated including the Morison elements of the pontoon, for wave steepnesses of 0.64% and 2% (magenta rhombus and orange squares, respectively). These results, on the one hand, make the effects of the non-linear drag on the resonant amplification clear (for periods above 24s); on the other hand, they also show that the cancelation point (period of zero heave motion slightly above 22s) expected from the potential flow analysis ceases to exist when the drag forces are considered. The same figure presents a set of experimental results obtained in regular wave tests (green triangles). All the experimental tests, for different wave periods, were conducted considering a fixed wave steepness of 2%. One may notice that the experimental results confirm the main trends obtained from the time-domain simulations. As expected, these experimental results attest that a proper consideration of the non-linear viscous effects is necessary for a good prediction of the resonant motions.

In general, therefore, the experimental results agree well with those obtained from the time-domain analysis. They attest that the viscous effects may indeed induce significant differences in the vertical motions of the platform for high wave periods. These differences include not only an attenuation of the resonant amplification (that can be emulated by means of external linearized damping) but also the suppression of the cancellation point of the RAO. The latter effect results from the differences in the hydrodynamic exciting force and cannot be reproduced by merely adding an external damping.

Since it is known beforehand that the heave motion is very important

for the prediction of wave amplitude, the problem of obtaining a proper representation of the heave RAOs becomes an important issue, especially considering the goal of estimating severe sea states with good accuracy. This is not straightforward task, considering the limitations imposed by the supposition of a linear dynamic model. For this reason, irregular wave tests with many of the extreme sea conditions (including 100yr conditions) were tested in the basin, aiming at quantifying the influence of the errors in the heave RAO model on the wave estimation. Moreover, two different approaches for defining the heave damping were tested, the first considering a mean value (independent of the heave amplitude), as presented in the frequency-domain results above; the second, with a simplified model that captures the variation of the linearized damping values as a function of the motion amplitude that is measured. This approach will be discussed in more details next.

### 4.3. Variable damping estimation

The reasons why a more refined damping model is needed for the heave motion were already pointed out. From the experimental data obtained during the decay tests, it can be observed that the damping factor is strongly correlated with the motion amplitude. Thus a method to account for this matter and obtain an estimation of the linearized equivalent external damping is needed.

A correction for the damping factor in the heave motion can be obtained as follows, using the Morison quadratic drag force formula (Morison et al., 1950):

$$F_D = \frac{1}{2}\rho S C_D \dot{z}|\dot{z}|, \tag{14}$$

the linearization of the drag force is obtained using the well-known method of equivalent energy dissipation (presented, for instance in Faltinsen (1993)) by means of an equivalent drag factor ($D^{\text{Equiv}}$). The drag factor ($D$) is linearized as function of frequency ($\omega$) and amplitude ($A$), obtaining that:

$$D^{\text{Equiv}} = \frac{8}{3\pi}\omega A D, \tag{15}$$

Then, the drag is rewritten as follows:

$$F_{D_L} = D^{\text{Equiv}}\dot{z} = D^{\text{Equiv}}\omega A. \tag{16}$$

Finally, the damping ratio can be expressed as:

$$\xi = \frac{\xi_{\text{Equiv}}}{\xi_{\text{Crit}}} = \frac{F_{D_L}}{2\omega_n M_T(\omega A)} = \frac{2}{3\pi}\rho C_D A \frac{l_{\text{pont}}\left(h_{\text{pot}} b_{\text{pot}}\right)}{(M + A_{33})}. \tag{17}$$

where $h_{\text{pont}}$ and $b_{\text{pont}}$ represents the height and the beam of the pontoon, respectively. $l_{\text{pont}}$ is the length of the pontoons in-between columns. $C_D$ represents the cross-sectional drag coefficient of the pontoon. $A_{33}$ is the heave added mass for the heave natural frequency and $M$ the total mass of the platform, whose sum is equal to $M_T$. Finally, $A$ stands for the representative amplitude of motion.

Therefore, with an appropriate value of $C_D$, an estimation of the heave external damping can be made based on a certain representative amplitude. In an irregular sea state, waves with different frequencies have different mean amplitudes. Nonetheless, for the purpose of estimating the damping, the most interesting frequency is the resonant frequency of motion. Keeping this in mind, an approximation for the representative amplitude of resonance heave motion ($A_H$) can be proposed as:

$$A_H = \sqrt{2S_H(\omega_n)\cdot\delta\omega_n} \tag{18}$$

where $S_H(\omega_n)$ is the power spectrum of the heave motion at the natural frequency and $\delta\omega_n$ is the frequency interval of the spectral analysis close to the natural frequency ($\omega_n$), or $[\omega_n - \omega_{(n-1)}, \omega_{(n+1)} - \omega_n]$. In section 5, the results of this analysis are confronted with the damping estimated from the experimental decay tests in heave, showing that a very good fit is obtained.

It should be noted that, since the heave amplitude $A_H$ can be obtained directly from the platform motion records, the procedure above can be used for pre-calibrating the damping level prior to each wave estimation event. In this way, the implementation is quite simple: all that is needed is a database of RAOs computed for different damping levels, defined within a specified range. At the moment of the wave estimation, the inference algorithm computes the heave motion amplitude and selects the most appropriate heave RAO for that particular estimation.

## 5. Experimental setup and tests performed

### 5.1. General

The model tests were carried out in the Numerical Offshore Tank (TPN) facilities, in the university of São Paulo (USP). The wave basin is a squared ($14.0m \times 14.0m \times 4.1m$) tank able to generate and absorb waves from 0.5Hz to 2.0Hz, by means of a set of 148 flap-type wavemakers. Fig. 6 shows a sketch of the wave basin and one of the horizontal mooring arrangements adopted during the experimental campaign.

The model was placed in the middle of the basin and its horizontal excursions were restricted by a soft mooring system. The campaign comprised only one draft (operational) and five wave headings from bow waves to beam waves (in this case: 180°, 150°, 135°, 120° and 90°). During the tests, the motions of the model were recorded with a Qualisys® optical tracking system.

### 5.2. Free floating decay tests

Decay tests were performed in still water for motions in the 6 DOF, in order to determine the natural periods and the damping characteristics of the semi-submersible platform model. For each motion, tests with four different initial amplitudes were carried out, with 3 repetitions each.

For avoiding spurious excitation of motions other than the ones being tested, a specific set up was used for the decay tests. This set up essentially comprised a set of bars and pulleys with a high resistance wire, used for moving the model and keeping it in the required initial position for each test. After releasing the model, all the motions were tracked by the Qualisys® optical system.

The method adopted for characterizing the non-linear damping in each test is essentially the one described in Faltinsen (1993), which considers a linear and a quadratic damping term. The former is supposed constant, while the later is expressed as a function of the motion

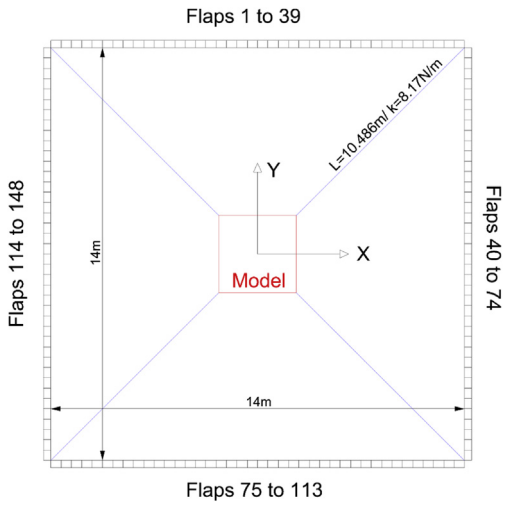


**Fig. 6.** Sketch of the wave basin and model (not in same scale), including the length and stiffness of the mooring lines.

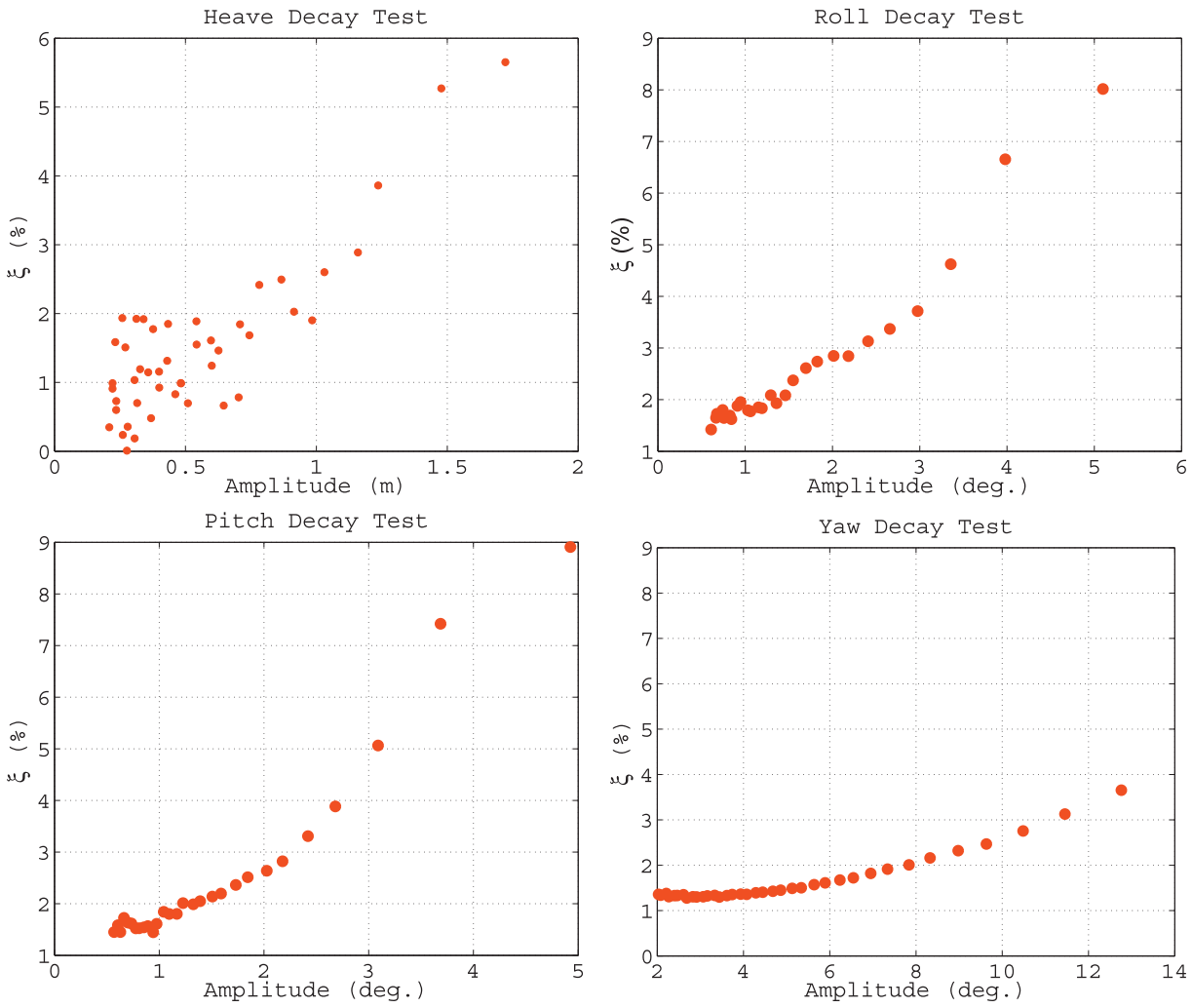


**Fig. 7.** Estimated damping ratios for heave, roll, pitch and yaw (from left to right and top to bottom).

amplitude. For illustration purposes, Fig. 7 presents the results obtained in tests for four different motions (namely, heave, roll, pitch and yaw). In this case, however, instead of presenting linear and quadratic damping coefficients, the results are combined and expressed in terms of the critical damping ratio for each amplitude.

### 5.2.1. *Variable damping model: a comparison with the results from decay tests*

Given the geometry of the semi-submersible platform, with the pontoons placed at relatively large depth, a comparison between damping estimations obtained from tests in waves and in calm water (decay tests) is illustrative. For doing this, the method proposed in the previous section for computing the heave damping from drag estimations was applied. The results were generated considering all the 32 different irregular waves tested in the wave basin. For each one of them, a representative resonant amplitude was obtained according to equation (18) and the damping ratio computed with equation (17). The damping ratios obtained from the irregular wave tests as a function of the resonant heave amplitudes may then be compared to the estimations derived from the decay tests (see Fig. 7). The agreement between the different methods is shown in Fig. 8, next. One may note that the damping ratio estimated from the irregular wave tests (black dots) indeed presents narrow differences with the linear fitting (red line) of the data obtained in the heave decay tests performed in calm water (blue triangles).

The small differences between the experimental results and the output of the variable damping model are attested by the comparison of

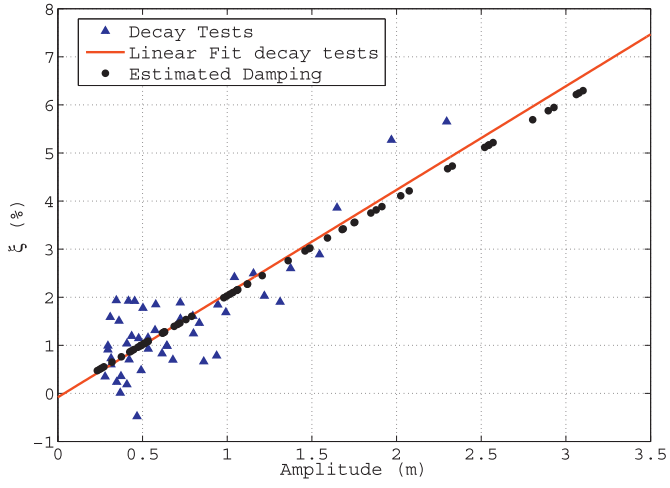


**Fig. 8.** Damping linearly estimated factor (black points) confronted with the experimental results presented in Fig. 7 (blue triangles) which are linearly fitted with the red line, for Heave motion. (For interpretation of the references to color in this figure legend, the reader is referred to the Web version of this article.)

**Table 2**
Linear ($p_1$) and quadratic ($p_2$) damping coefficients given by the experimental results and the estimations obtained with the variable damping model.

| | Experimental | Model |
|---|---|---|
| $p_1$ | $-1.0e-4$ | $2.0e-17$ |
| $p_2$ | $2.2e-2$ | $2.0e-2$ |

the linear and quadratic damping coefficients. The values of these coefficients have been obtained following the procedure proposed by Faltinsen (1993), which assumes that the motion can be written as:

$$\ddot{x} + p_1\dot{x} + p_2\dot{x}|\dot{x}| + p_3 x = 0, \tag{19}$$

By fitting the results obtained in the decay tests and those of the damping model according to this procedure, the coefficients obtained are given in Table 2, where the linear damping coefficient is named $p_1$ and the quadratic damping coefficient is given by $p_2$.

Despite the differences in the linear coefficient, it is clear that the damping is dominated by the quadratic term, especially for the larger amplitudes/velocities of motion. The agreement regarding $p_2$ is indeed remarkable, once again attesting the conclusions derived from the graphical representation of the results.

The good agreement obtained with the variable damping model also attests that the heave damping is dominated by the platform motions and that the effects of the wave induced flow on the damping force are indeed small, even for the largest wave amplitudes that were tested. In this sense, the good fit with the decay data indicates that the method proposed represents a proper means of estimating the resonant heave damping in waves.

### 5.3. Wave tests

#### 5.3.1. Transient and regular wave tests

Transient wave tests were used to verify the accuracy of the motion RAOs obtained with the numerical model. For this reason, the wave steepness was kept below 4% during all the tests. The range of periods for the generation of the transient waves was set from 8 to 24 s (in real scale), with a constant wave amplitude equal to 1.68*m*. These tests had a full-scale equivalent duration of 240 s, thus comprising at least ten waves cycles for each condition.

In addition, a set of 33 tests in regular waves was carried out for a better evaluation of the non-linear effects on the RAOs. Again, the wave period ranged from 8 to 24 s, but different wave amplitudes were tested considering wave steepness of 2%, 4% and 6%.

Fig. 9 illustrates the level of agreement obtained between the motion RAOs derived from the wave tests (both for transient and regular waves) and those derived numerically. Results correspond to a wave heading of 135deg. and comprise only the three motions that were used for the purpose of wave inference (heave, roll and pitch). It can be seen that the agreement for the angular motions is good for the whole range of frequencies. As mentioned before, this was indeed expected because neither roll or pitch resonate in the wave frequency range. For the heave motion,

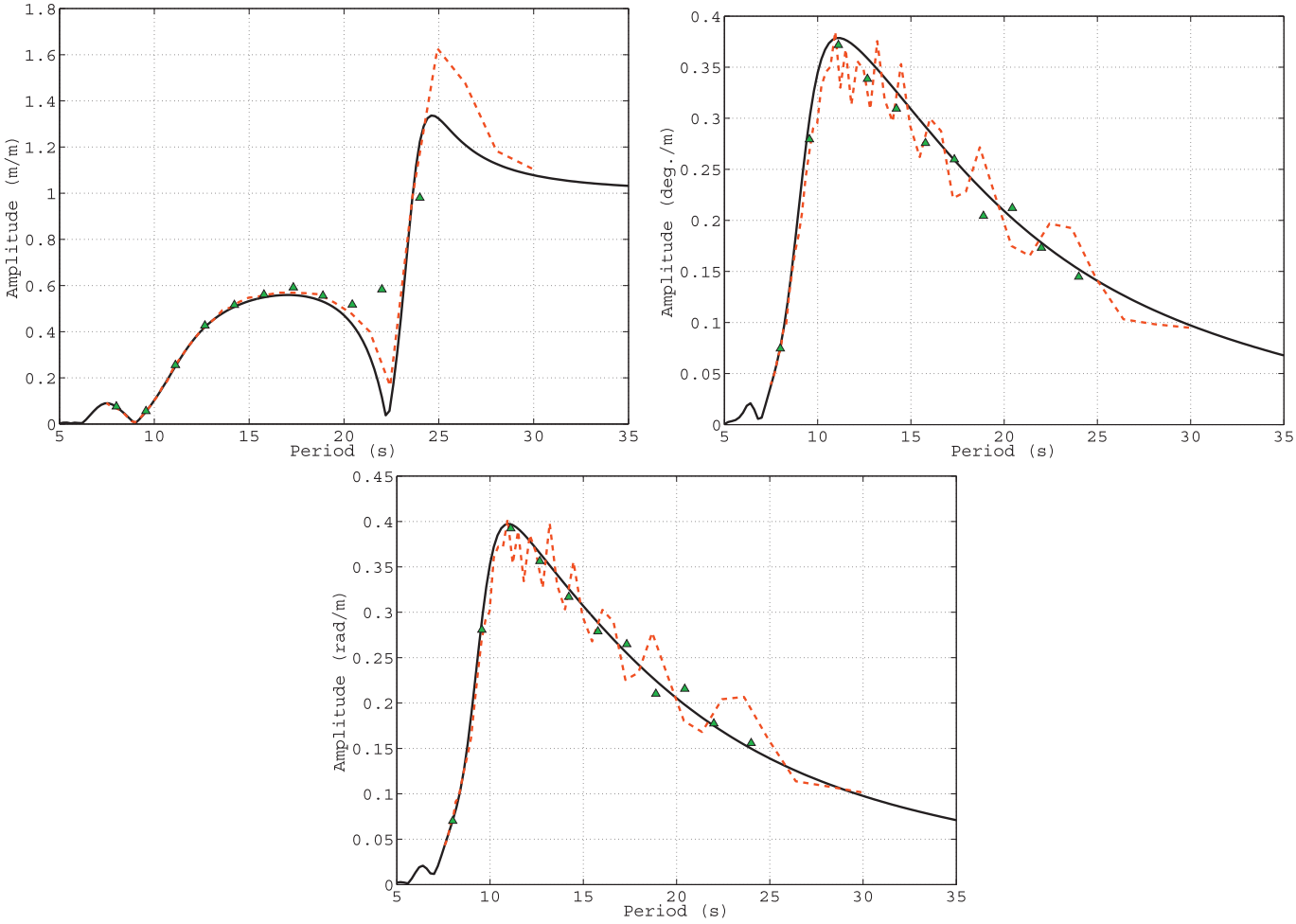


**Fig. 9.** Comparison of the (heave, roll & pitch) RAOs estimated numerically (black line) with the experimental results, both transient (red dashed line) and regular waves with 2% of steepness (green triangles), for the heading of 135°. (For interpretation of the references to color in this figure legend, the reader is referred to the Web version of this article.)

on the other hand, the agreement is good for wave periods up to 20 s. As anticipated in section 4.2, discrepancies rise for larger periods and are associated to viscous effects within the resonant range.

Regarding the use of the heave motion for wave inference, part of these discrepancies will be mitigated with the use of a proper damping model, which should provide a better adjustment of the resonant amplification for wave periods around the natural one. Another source of error, however, namely the one related to the motions observed closer to the numerical cancellation point, are more difficult to mitigate when using the linear frequency-domain results.

#### 5.3.2. *Irregular wave tests*

The selection process of irregular waves (sea states) was based on the wave statistics for the Åsgard field, in the Norwegian sea (from Mathiesen and Nygaard (2013)). A set of 32 sea conditions with corresponding peak periods ($T_p$) and significant wave heights ($H_s$) was selected (see Table 3), ranging from mild waves with high probability of occurrence to extreme 100yr-return events. Following the recommendation proposed in Torsethaugen et al. (2004), for a proper representation of each sea condition, the limiting spectral peak period (defined by the relation $T_{p_f} = 6.6H_s^{1/3}$) was estimated using the theoretical significant wave height value. Then, if the expected peak period of the sea ($T_p$) was located within a band given by $T_{p_f} \pm 2$ seconds, the JONSWAP standard model was adopted to generate the spectrum; otherwise, the spectrum was generated using the Torsethaugen spectrum. Fig. 10 provides a comparison between the Torsethaugen spectrum and an equivalent JONSWAP spectrum for the same significant wave height and peak period. One should note that the Torsethaugen spectrum is a bimodal sea spectrum composed by a swell (energy around the peak in the low frequency range) and a wind sea (energy components given in the high frequency range).

#### 5.3.3. *Wave calibration*

Wave calibration tests were performed in the absence of the semi-submersible model and the evaluation of the wave spectrum within the test zone was performed by means of an array of three wave probes. The quality of the waves generated in the basin was checked considering the main statistical parameters. Each condition was repeated at least twice. In this calibration procedure, the maximum frequency of the spectrum was 2Hz, corresponding to 5.5 s in full-scale. The procedure has guaranteed that errors in the values of $T_p$ and $H_s$ were lower than 5% for all tests.

**Table 3**
Input parameters used for all the sea tests conditions.

| Wave ID | Sea Spectrum | $H_s(m)$ | $T_p(s)$ | Wave Steepness (%) |
|---|---|---|---|---|
| STA-IRR-01 | JONSWAP | 3,50 | 9,50 | 2,48 |
| STA-IRR-02 | JONSWAP | 3,50 | 11,50 | 1,70 |
| STA-IRR-03 | TORSETHAUGEN | 3,50 | 13,50 | 1,23 |
| STA-IRR-04 | TORSETHAUGEN | 3,50 | 15,50 | 0,93 |
| STA-IRR-05 | TORSETHAUGEN | 3,50 | 18,50 | 0,65 |
| STA-IRR-06 | JONSWAP | 4,50 | 10,50 | 2,61 |
| STA-IRR-07 | JONSWAP | 4,50 | 12,50 | 1,84 |
| STA-IRR-08 | TORSETHAUGEN | 4,50 | 14,50 | 1,37 |
| STA-IRR-09 | TORSETHAUGEN | 5,50 | 9,50 | 3,90 |
| STA-IRR-10 | JONSWAP | 5,50 | 11,50 | 2,66 |
| STA-IRR-11 | JONSWAP | 5,50 | 13,50 | 1,93 |
| STA-IRR-12 | TORSETHAUGEN | 5,50 | 18,50 | 1,03 |
| STA-IRR-13 | JONSWAP | 6,50 | 12,50 | 2,66 |
| STA-IRR-14 | TORSETHAUGEN | 6,50 | 16,50 | 1,53 |
| STA-IRR-15 | JONSWAP | 7,50 | 11,50 | 3,63 |
| STA-IRR-16 | JONSWAP | 7,50 | 13,50 | 2,64 |
| STA-IRR-17 | TORSETHAUGEN | 7,50 | 18,50 | 1,40 |
| STA-IRR-18 | JONSWAP | 8,50 | 12,50 | 3,48 |
| STA-IRR-19 | JONSWAP | 9,50 | 12,50 | 3,89 |
| STA-IRR-20 | JONSWAP | 9,50 | 14,50 | 2,89 |
| STA-IRR-21 | TORSETHAUGEN | 9,50 | 16,50 | 2,23 |
| STA-IRR-22 | TORSETHAUGEN | 9,50 | 18,50 | 1,78 |
| STA-IRR-23 | JONSWAP | 10,50 | 14,50 | 3,20 |
| STA-IRR-24 | JONSWAP | 11,70 | 14,00 | 3,82 |
| STA-IRR-25 | JONSWAP | 11,70 | 15,70 | 3,04 |
| STA-IRR-26 | TORSETHAUGEN | 11,70 | 18,10 | 2,29 |
| STA-IRR-27 | JONSWAP | 14,10 | 15,70 | 3,66 |
| STA-IRR-28 | JONSWAP | 14,10 | 16,90 | 3,16 |
| STA-IRR-29 | TORSETHAUGEN | 14,10 | 19,30 | 2,42 |
| STA-IRR-30 | JONSWAP | 16,40 | 16,90 | 3,68 |
| STA-IRR-31 | JONSWAP | 16,40 | 18,10 | 3,21 |
| STA-IRR-32 | TORSETHAUGEN | 16,40 | 19,50 | 2,76 |

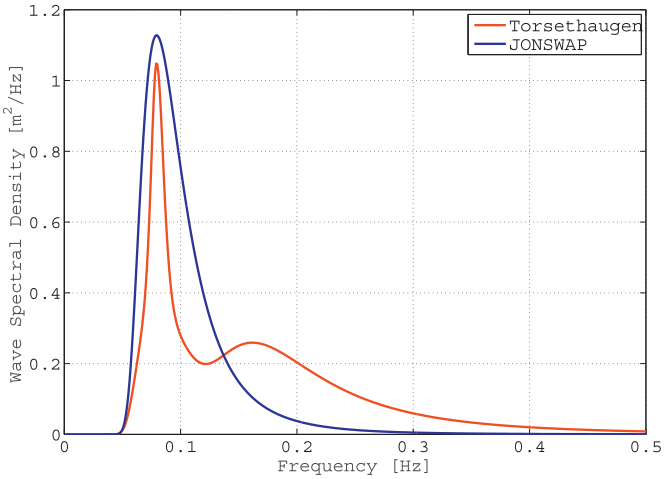


**Fig. 10.** JONSWAP and Torsethaugen spectrum for $H_s = 1$m and $T_p = 12.6$s.

#### 5.3.3.1. *Experimental measurements of the directional wave spectrum.*

In order to provide a reference for evaluating the accuracy of the sea conditions estimated using the motion-based wave inference algorithm, an array of eight wave probes has been used to measure the directional wave spectrum in the CH-TPN basin in the absence of the semi-submersible model. The procedure adopted to measure directional waves follows the one proposed by Nwogu (1989), applying the Maximum Entropy Method (MEM). A good explanation of the procedure adopted for estimating the spectrum from the wave records can be found in Tannuri et al. (2007). The disposition of the wave probes is similar to the one proposed in Stansberg et al. (1998), with six wave probes placed in the vertices of a regular hexagon with a circumradius equal to 0.4m, plus two central ones. Fig. 11 provides a view of the wave probes arrangement installed in the basin.

For illustrative purposes, Fig. 12 presents the results obtained with MEM method for the irregular waves generated in four different tests, which were selected among the 32 tests in order to provide a representative sample of the whole range of periods that was tested. In these polar plots, the wave energy in each wave frequency (radial coordinate in rad/s, with values given in real scale) is depicted for all wave directions (as a convention, the wave direction in the tank was considered as 180deg). In addition, the main statistical parameters for each wave condition are presented at the top of each figure. It should be stressed that, instead of the peak period, the mean central period $T_1$ will be used for evaluating the results. The reasons for that are explained in the next section.

All waves generated in the basin were long-crested, meaning that no directional energy spread was considered in the wave generation. For this reason, one may realize that the wave spectra measured with the MEM method have energy concentrated in a very narrow range around the mean direction (the directional resolution considered in the spectral analysis corresponded to $\Delta\theta = 5$deg, the same that was employed for the motion-based wave inference, whose results will be presented next).

## 6. Results: wave inference based on the motions of the model

In the following, the main results obtained with the wave inference method based on the motions of the semi-submersible model are

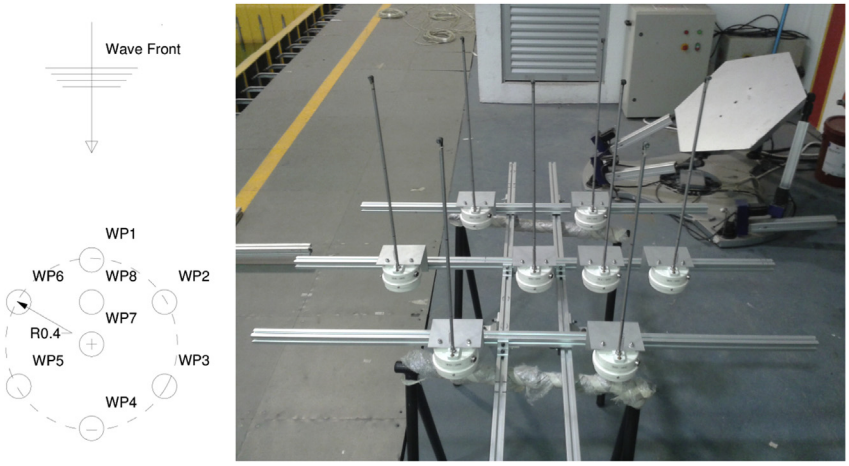


**Fig. 11.** Lay-out of the wave probes array and picture of the array before the installation in the wave basin.

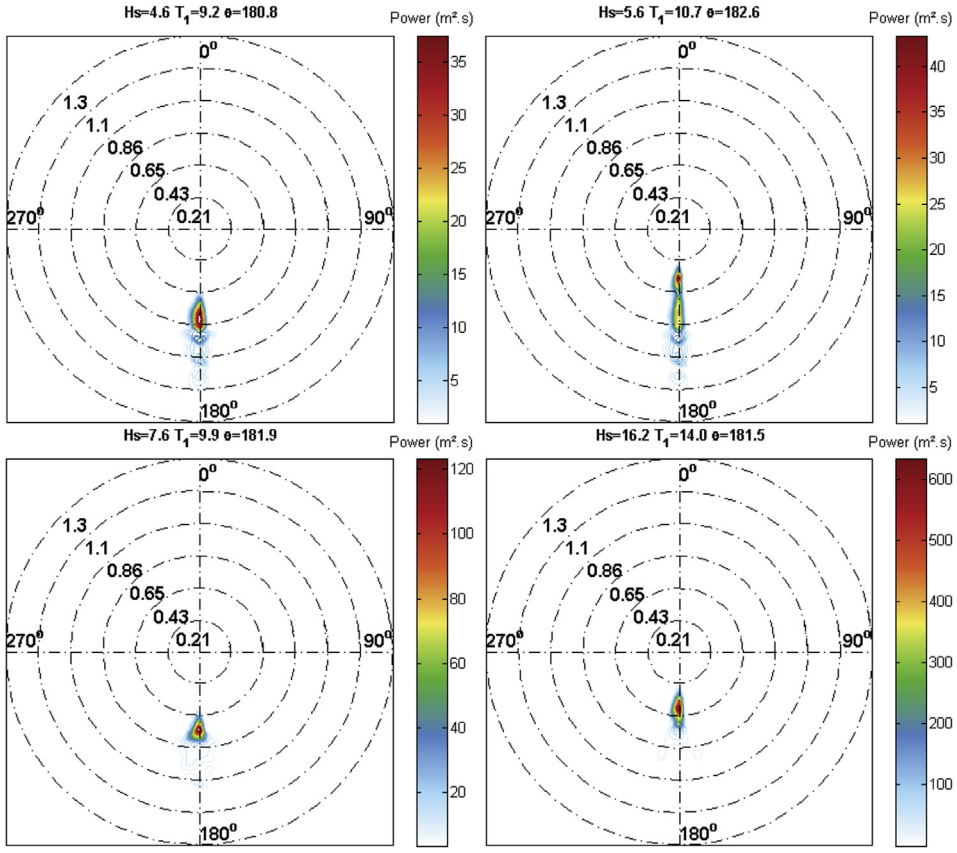


**Fig. 12.** Irregular sea estimation using MEM for the tests: 6, 12, 15 and 30 (full-scale).

presented and confronted to the measurements performed in the wave basin with conventional wave probes.

It is worth remembering that the motion basis adopted for the analysis comprised only three motions, namely heave, roll and pitch. The mathematical algorithm was implemented in MATLAB® 2014a. Twenty different wave frequencies were considered, with a spatial resolution of $\Delta\theta = 5$ degrees (corresponding to $M = 20$ and $K = 72$, see section 2). Moreover, three different sets of RAOs were employed as alternatives for modelling the heave motions: one with a constant external damping coefficient corresponding to 5% of the critical damping, a second one obtained with the variable damping method computed according to the procedure presented in section 4 and, also, the RAOs obtained with the time-domain analysis considering the pontoon drag forces (see Fig. 5).

Regarding the values of the hyperparameters, an extensive error analysis was carried out to determine the most favorable values. As a result, the calibration of $u_1$ was made based on the period of the motions, according to the procedure defined by Bispo et al. (2012), whereas for $u_2$ the best value was given by $1{\cdot}10^{-5}$ and for $u_3$ it was equal to 0.0035. With this set of input parameters, the mean computational time required for the estimation of one wave condition, using a conventional desktop PC, was around 30 s.

For all the results showed ahead, the motion-based wave estimations

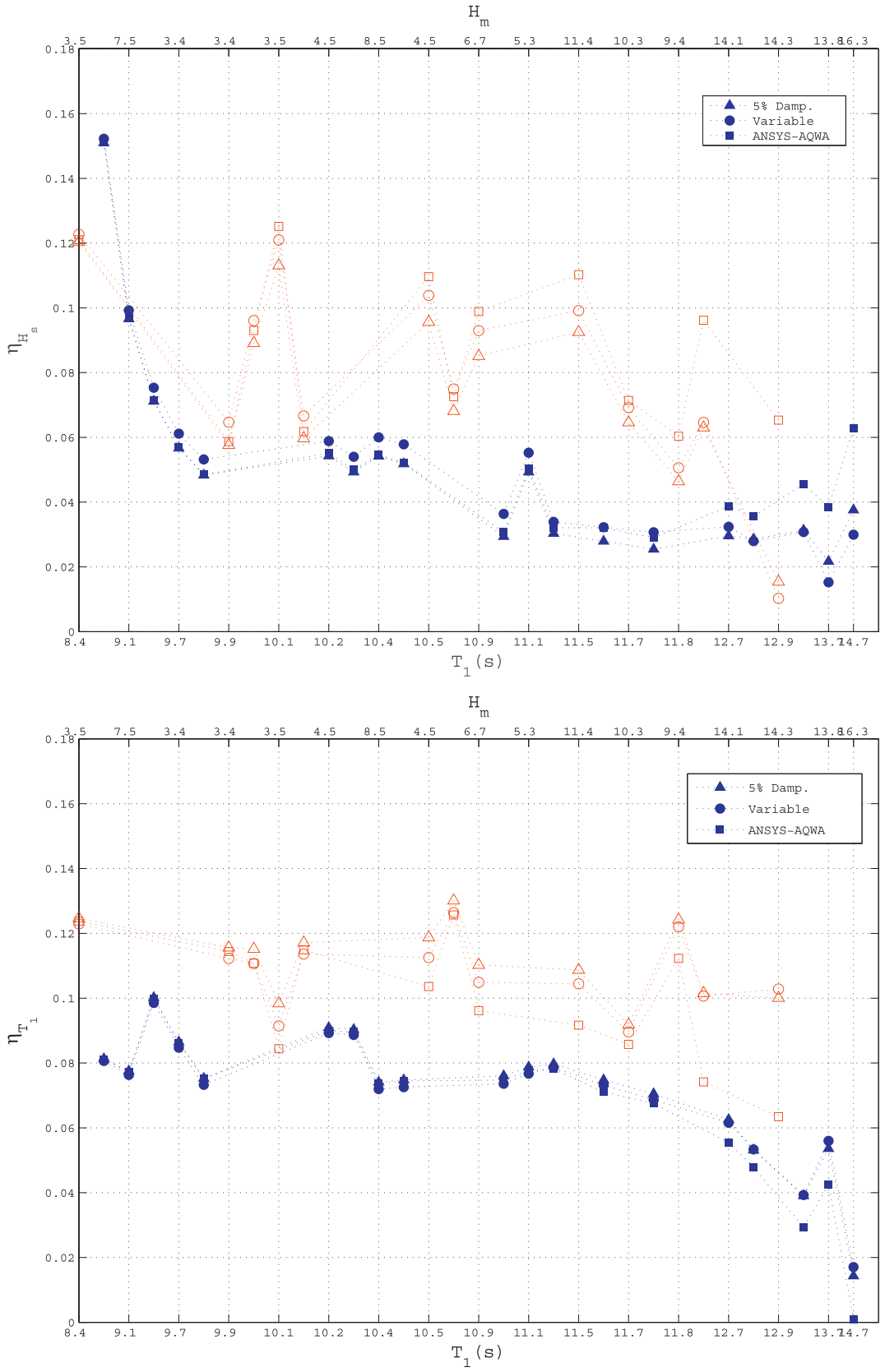


**Fig. 13.** Results of the wave inference method with constant and variable damping factor for the heading 90°. These figures refer to the relative values of the significant wave height and the mean centroid wave period. Empty and blue markers stand for the Torsethaugen and JONSWAP spectrum respectively. (For interpretation of the references to color in this figure legend, the reader is referred to the Web version of this article.)

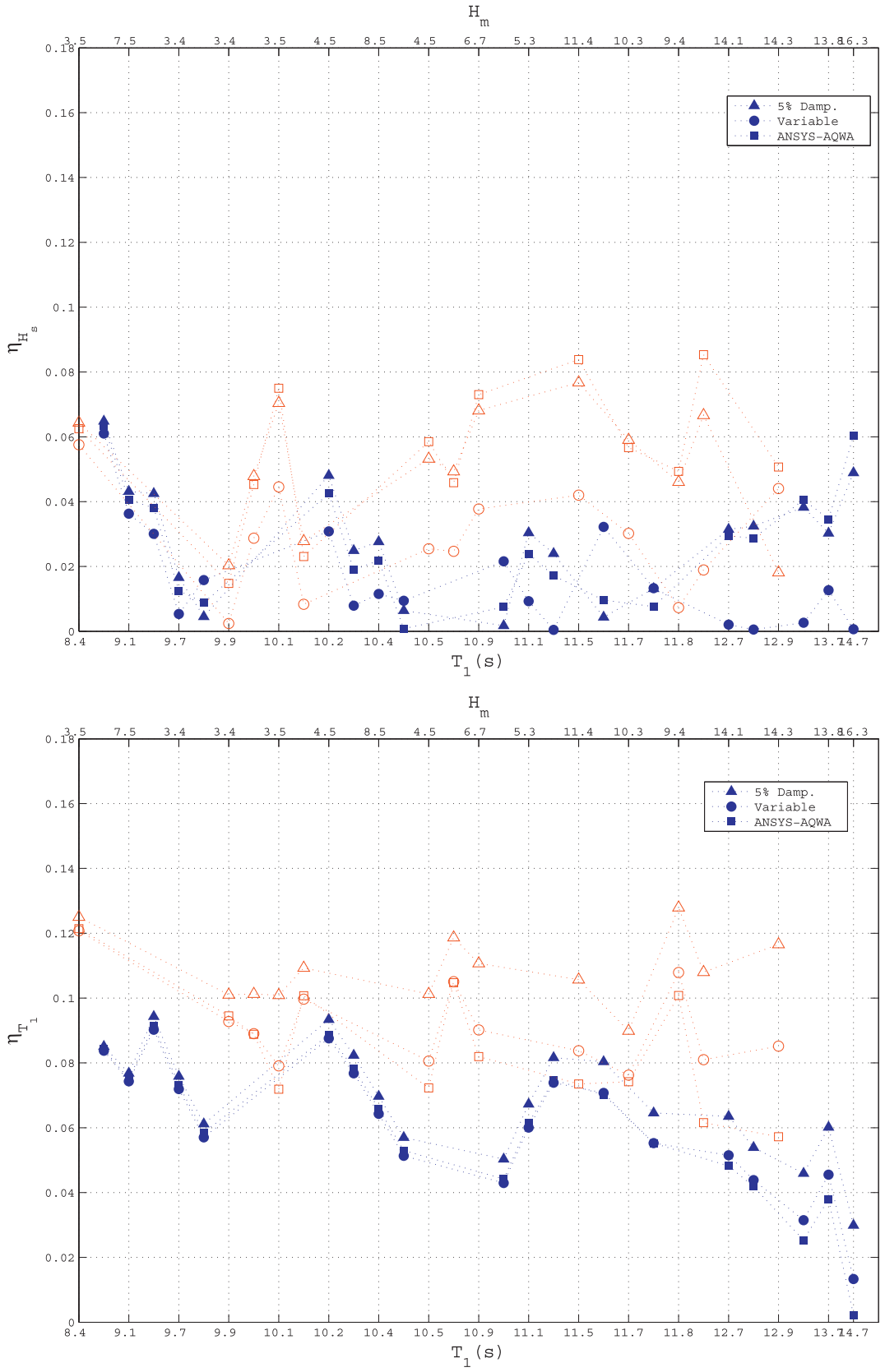


**Fig. 14.** Results of the wave inference method with constant and variable damping factor for the heading 135°. These figures refer to the relative values of the significant wave height and the mean centroid wave period. Empty and blue markers stand for the Torsethaugen and JONSWAP spectrum respectively. (For interpretation of the references to color in this figure legend, the reader is referred to the Web version of this article.)

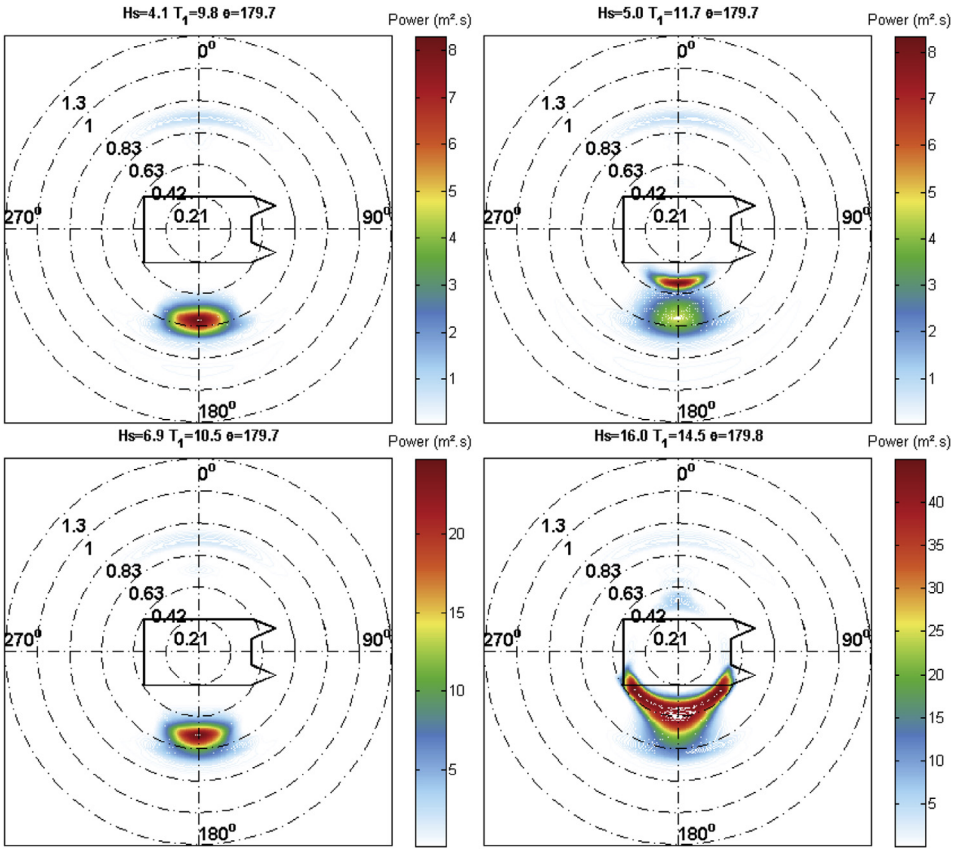


**Fig. 15.** Wave spectra estimated using variable damping for the heading 90°.

have been made considering the first 30 min of data acquisition,[1] period of time that is typically assumed as the length of the stationary period (e.g. Soares and Fricke (2011)).

In Fig. 13 and Fig. 14 the reliability of the estimations was evaluated by means of relative errors. Accordingly, the vertical axes of these figures provide the relative errors for the following statistics:

- Significant wave height ($H_s$), that leads to the following relative error,

$$\eta_{H_s} = \frac{|H_m - H_s|}{H_m}, \tag{20}$$

where $H_m$ stands for the significant wave height obtained from the measurements in the basin (with wave probes) and $H_s$ is the value of the significant wave height estimated by means of the motion-based method;

- Mean wave period ($T_1$), which relative error is given by,

$$\eta_{T_1} = \frac{|T_m - T_1|}{T_m}, \tag{21}$$

where $T_m$ is the mean wave period measured in the basin and $T_1$ is the value estimated with the motion-based method. It must be emphasized, once more, that the platform is expected to filter certain part of the energy placed in high frequency range. For this reason, $T_1$ has been adopted as a reference for the errors instead of $T_p$, obtaining a better indicator of the distribution of the energy in the different frequencies.

The relative errors in the wave statistics are presented as a function of the (measured) mean period ($T_1$) of the waves in each test, given in the lower horizontal axis. The upper axis indicates the corresponding (measured) significant wave heights, in meters. In this way, the reader can assess the agreement obtained with the motion based method for different wave periods and heights. Moreover, it should be noticed that these figures present three sets of results, that correspond to the estimations obtained using the different RAOs described above. Finally, it must be realized that the results are clustered into two different sets with different colors, indicating whether the waves generated in the basin corresponded to a JONSWAP (blue) or Torsethaugen (empty-red) power spectrum.

The figures referred above only include information for waves coming from 90° and 135°, because other headings conditions tested during the experimental campaign did not provide any meaningful new information (see Fig. 19).

Fig. 15, next, presents a polar plot for the directional wave spectra estimated in a few selected cases among the beam sea tests. Once again, the results include conditions that are representative of cases with low and high peak periods (for an easier comparison, the maps correspond to the same sea states presented before in Fig. 12). In this figure, the accuracy regarding the estimation of the mean wave direction ($\theta$) can be assessed (reminding that the expected wave direction in the tank is 180°). In addition, one may also evaluate the results in terms of the energy spreading, both in frequency and direction. Fig. 16 provides the same results for the tests with quartering sea conditions (heading of 135°).

Figs. 17 and 18 show the 2D wave spectra estimated (dashed blue line) for sea conditions 6, 12, 15 and 30 (see Table 3). Also, aiming at providing a reference for the posterior analysis, the sea spectra obtained from the wave probes records are also included in these figures (black lines).

In addition to the graphical results, Table 4 provides the mean values of the errors obtained not only for beam and quartering wave conditions, but also for the other wave headings adopted in the tests. It presents the mean relative errors for significant wave height, mean wave period, peak period and also the absolute error of the estimated direction. It should be

[1] Time span that assures that a minimum number of 200 wave cycles are used to estimate the wave conditions, as suggested in ITTC (2014).

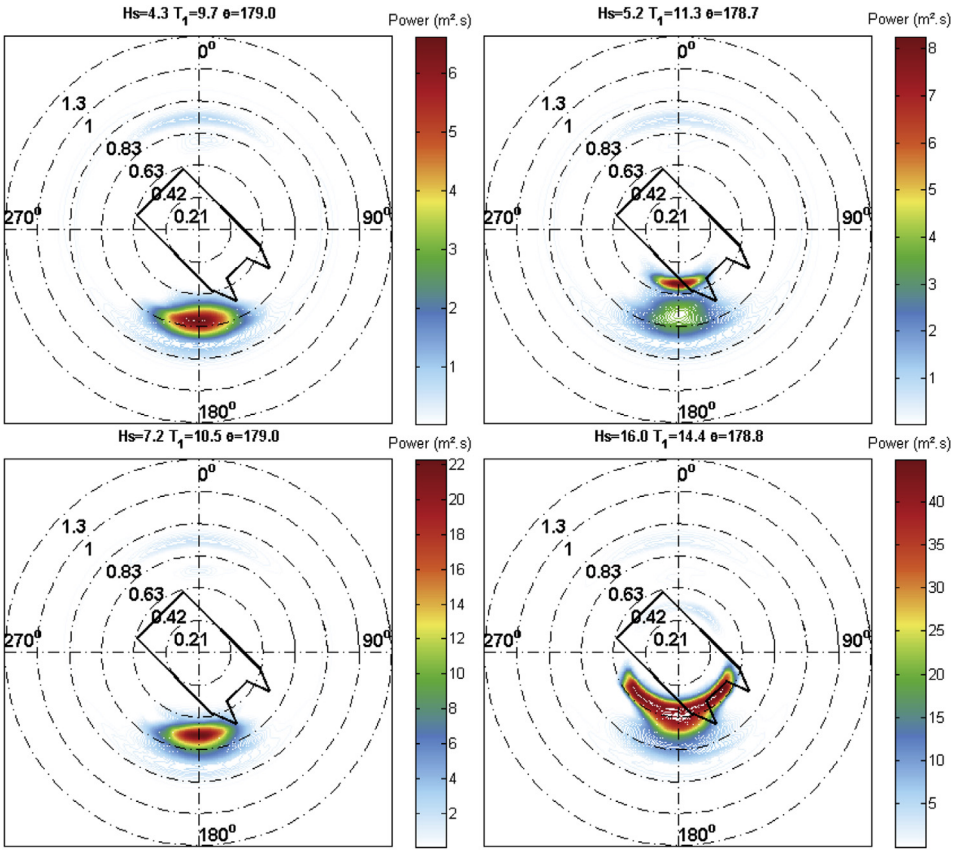


**Fig. 16.** Wave spectra estimated using variable damping for the heading 135°.

realized that the results displayed for each heading combines all the tests within a certain range of peak wave period. This was made in order to allow an easier evaluation of how the errors behave as the wave period changes. Finally, the results are presented separately for JONSWAP and Torsethaugen spectra.

The presentation of the results is concluded with Fig. 19, that was conceived in order to provide a practical way for the analysis involving the five different headings and all the 32 different sea conditions tested during the experimental campaign. In this case, once again, only the results with the variable damping method are presented. Moreover, one may infer not only the mean errors and how they change with the wave period, but also the variations induced by the different wave headings.

Based on these figures and on the results in Table 4, a detailed discussion of the performance of the motion-based method will be presented next.

### 6.1. Discussion

Many aspects of the results presented above deserve attention. First, by inspecting the error statistics obtained with the wave inference method (Table 4), it can be concluded that the overall agreement with the expected values is indeed very good for all the different headings. Considering the whole range of wave periods tested, the maximum errors involved in the prediction of wave height and mean wave period are around 10% for JONSWAP seas, and 15% for the conditions corresponding to the bimodal Torsethaugen spectra.

Regarding only the significant wave height, the inference method usually underestimates the experimental values, the errors being below 16% for the most unfavorable headings (90° and 180°) and below 7% for the most favorable one (135°). It must be stressed that the underestimation observed is indeed consistent with the expected bias of the method, since part of the energy in the high frequency wave components is filtered as these waves do not impose motions of the hull. It is also important to observe that the level of underestimation and the differences between the headings tend to decrease as the wave period increases, favoring the results for the most severe sea states. This trend can be readily attested by observing the variation of the errors in Fig. 13 and also by comparing the errors for different period ranges in Table 4.

The results obtained for the predicted mean wave periods ($T_1$) are also consistent with the bias of the method. Since energy is filtered from the wave components with higher frequencies, the mean frequency of the estimated spectrum tends to be lower than the real one and, consequently, the mean period tends to be higher. Nonetheless, the results show that differences are not large, the errors being always below 15%. Once again, the errors decrease for larger wave periods, as should be expected. On the other hand, Table 4 also provides the relative error concerning the estimated peak period ($T_p$). The results show that the peak period is always estimated accurately, with an error below 4%. Another important characteristic of these estimations is that there is no significant variation between the outputs obtained with different headings and for different wave periods, attesting that the prediction of ($T_p$) is less sensitive to these factors.

Figs. 13 and 14 also allow an assessment of the influence of the different heave RAO models on the motion-based predictions. It is interesting to realize that the main influence arising from the consideration of pontoon drag effects occurs in the estimation of the significant wave height. Neither the mean wave direction nor the mean wave period are substantially changed by the use of alternative RAOs. Moreover, one may realize that the discrepancies in the wave height predicted by the different models increase for larger periods. This was already expected and happens due to the fact that these waves induce resonant heave motions that are more pronounced. For the larger periods, results indicate that the variable damping model provided the smallest errors in the wave height, if compared to the other models that were tested (constant damping or the RAOs corrected by means of time-domain simulations).

Regarding the shape of the wave spectrum, the relative errors (for

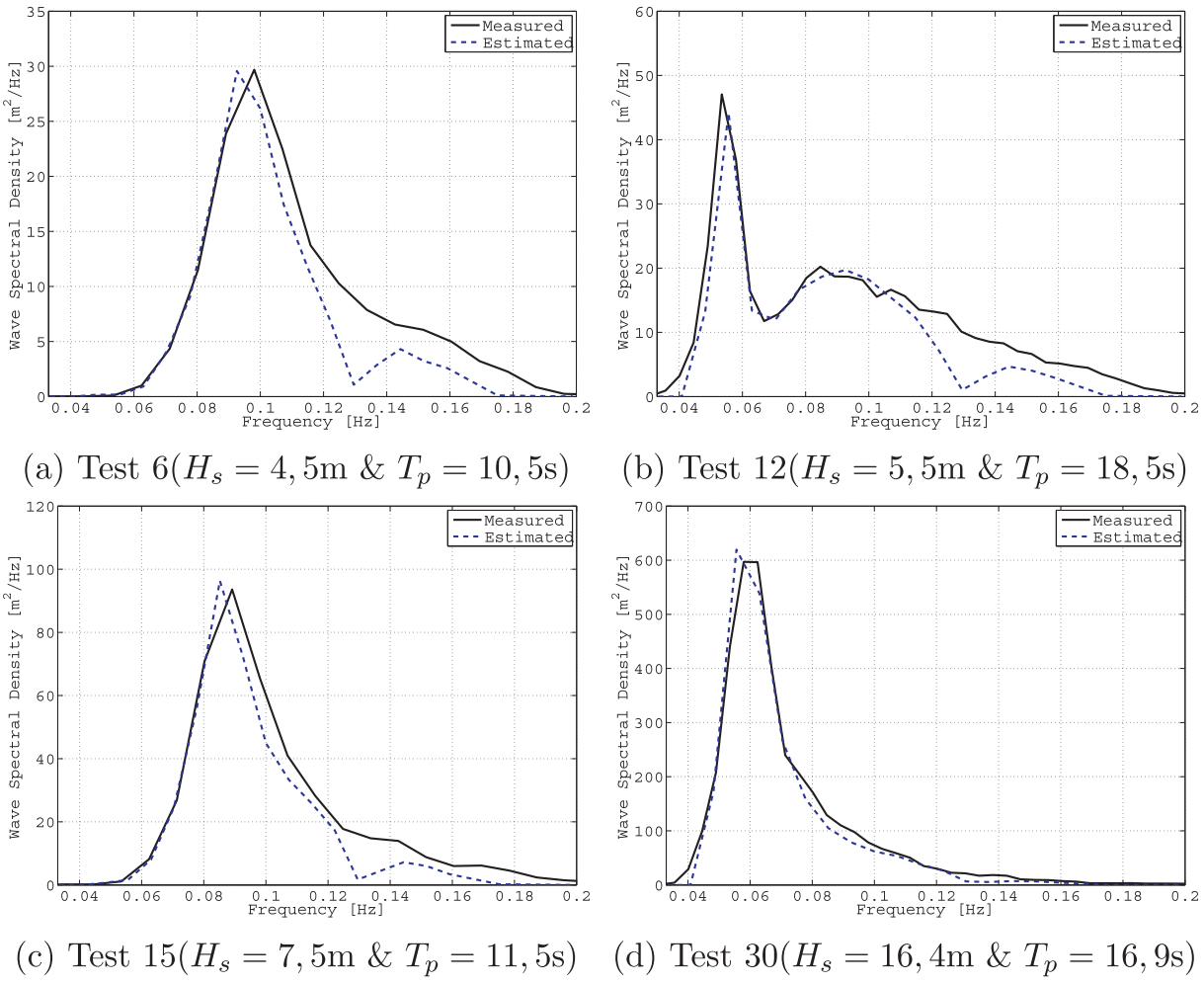


**Fig. 17.** Comparison between the estimated sea spectrum and the measured by means of an array of conventional wave probes, for the heading 90°.

significant wave height and mean period) are amplified by Torsethaugen model for all the wave headings. Again, this is not surprising since, compared to the JONSWAP model (see Fig. 10), the Torsethaugen spectrum places a larger amount of energy in the high frequency range, in which the dynamic response of the model is less pronounced. Figs. 17 and 18 reflect this filtering effect in the high frequency range, for both heading conditions. Furthermore, both figures show an example of a 100yr condition (test case 30) which attests that for the most extreme conditions only a small amount of energy is filtered from the sea spectrum, due to the large peak periods typically observed in these situations. Regarding the energy distribution in the frequency range, one may realize that it changes according to the wave heading, resulting in the variations of the estimations of $T_1$ showed in Table 4. Nevertheless, as mentioned before, the peak period is always captured correctly by the method.

Furthermore, the whole set of results shows that the most unfavorable headings are those of bow (180°) and beam (90°) waves. Once again, this was expected because these are the situations when only 2 of the 3 motions used for the estimations are excited by the waves (for the 180° heading, there are no significant roll motions; for the 90° heading there are no significant pitch motions). On the other hand, the most favorable conditions are those closer to 135 (or 45) degrees, when all the 3 motions are excited and thus the amount of information available for the estimations is larger.

When the mean wave direction is concerned (see Figs. 15 and 16), although the estimated spectra present a somewhat larger spreading of energy if compared to those obtained from the wave probes (see Fig. 12 for a proper comparison), the prediction of the mean direction was very accurate for all the conditions tested. This is because only long crested sea conditions were tested during the experimental campaign. In short crested seas, one may expect that the filtering effects of the platform dynamics on the high frequency energy components, may, in some cases, lead to poorer estimations of the mean wave direction. On the other hand, the larger spreading of wave energy observed when using the Bayesian inference method is related to the calibration of the hyperparameter $u_1$, which controls the level of smoothness of the spectrum with respect to the wave direction. In this case, the pre-calibration of the hyperparameter was made seeking to improve the accuracy in the prediction of the main statistical wave parameters ($T_1$ and $H_s$), a procedure that ultimately led to a somewhat larger wave spreading. This trade-off between accurate energy predictions and smoothness of the spectrum is a particular feature of the present version of the Bayesian inference method. At the present moment, an investigation on alternative prior distributions is being made, as an attempt of improving this trade-off. However, in face of the good results obtained so far, this is considered to be a secondary aspect.

Finally, to conclude the discussion of the main aspects, some additional comments regarding the prediction of the most extreme conditions must be made. In fact, it is important to realize that the 100yr wave conditions could be captured by the motion-based method with errors lower than 5% in both wave height and period (for the JONSWAP model). These conditions involved waves with $H_s$ over 16 m and peak periods close to 20 s. Obviously, one must remind that these good results were obtained in model scale, in very controlled conditions. When

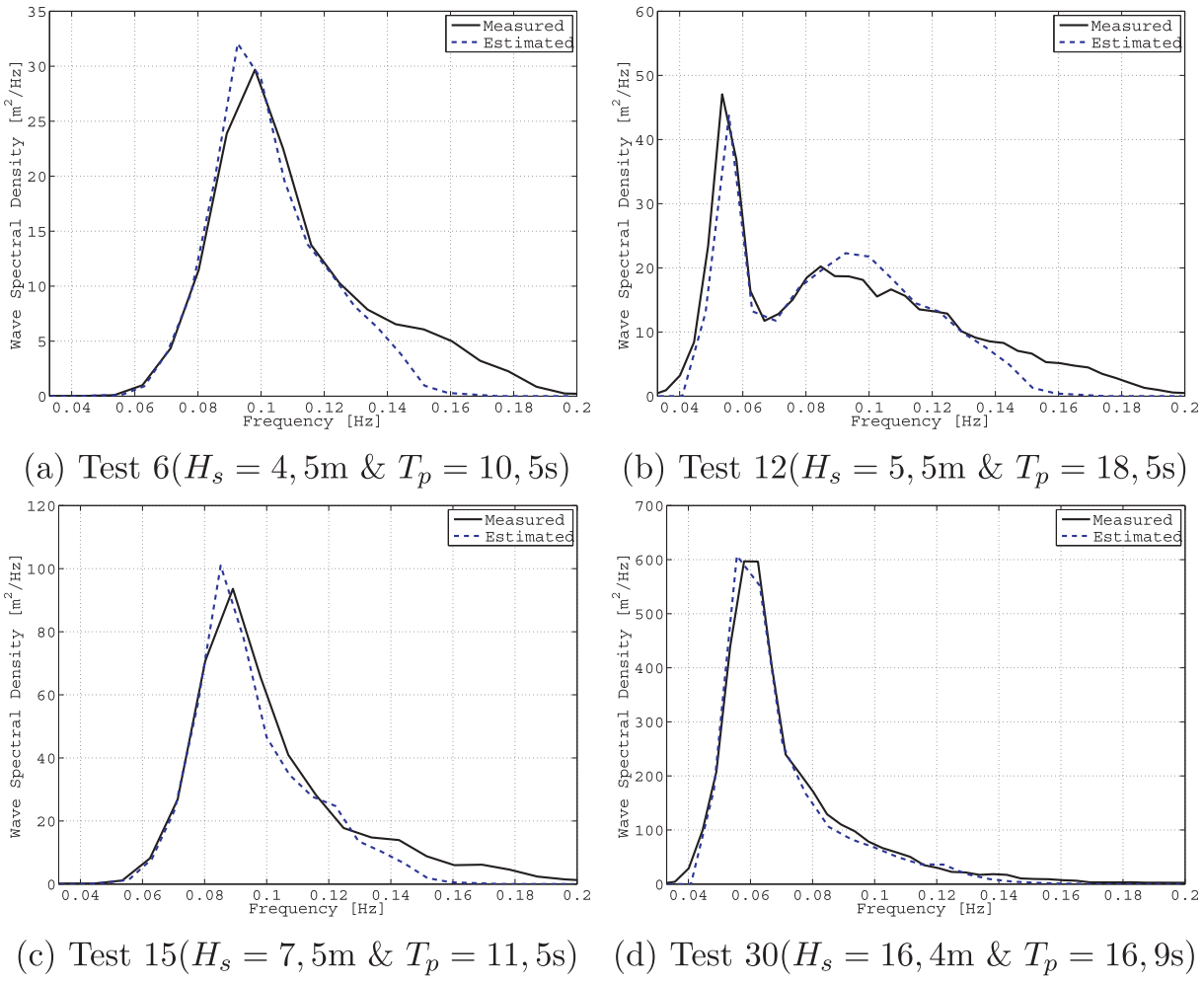


**Fig. 18.** Comparison between the estimated sea spectrum and the measured by means of an array of conventional wave probes, for the heading 135°.

considering the estimations made aboard a real unit, other factors like the presence of risers and mooring lines and the effects of wind and current on the motions, for example, will certainly impose a more demanding scenario for the predictions. Nonetheless, the favorable results obtained in the tests are certainly promising enough to motivate the continuity of the research, during which these other factors must be properly addressed.

## 7. Conclusions

An experimental study about the usefulness of employing a semi-submersible platform for motion-based estimations of local sea spectrum was presented and the results were evaluated by means of an extensive set of model-scale tests performed in a wave basin. For this purpose, a (1 : 120) scale model of a semi-submersible unit has been tested in five different headings, comprising waves that ranged from typical to severe wave conditions representative of the Åsgard field, in Norway. Waves were generated considering both, unimodal (JONSWAP) and bimodal (Torsethaugen) spectral models. The directional wave spectra estimated from the model motions were directly confronted to the experimental measurements obtained by means of conventional wave probes.

A Bayesian inference model with three hyperparameters (as proposed by Simos et al. (2012)) was adopted for the estimations. This method includes the addition of a third hyperparameter, which indeed improved the results, compared to those obtained with only two hyperparameters. The predictions considered a basis composed of three motions (heave-roll-pitch), which proved to be appropriate for all the sea conditions tested.

Results have shown that all the wave conditions tested could be accurately inferred from the Bayesian method, keeping the errors below reasonable limits. The errors were larger in the most unfavorable conditions, which correspond to the ones with small motions (small periods or mild seas) and in the cases when the sea only excited two of the three motions (bow and beam waves). The errors are reduced in the cases were the platform presents larger motions, or provide more information, which were given when the heading was close to 135° and for the more severe wave conditions (when the wave induce more pronounced motions). All the results confirmed the expected biases of overestimating the wave period while underestimating the wave height, deviations that are progressively smaller as the wave period increases.

The analysis of the results with RAOs obtained from different approaches also highlighted the importance of a proper modelling of transfer functions of motion. In the experimental setup, a soft mooring system was used and the major source of drag was the platform itself. In this condition, the results obtained when using the variable external damping method (a damping ratio proportional to the recorded heave amplitude in each test) proved to be a good option for dealing with effects of the non-linear viscous damping.

So far, as a general conclusion, one may state that the results obtained with the small-scale tests indicate that semi-submersible platform indeed may be considered as a good choice for the motion-based wave inference. In addition, the results for more severe sea states are promising, even when the RAOs are modeled in a conventional linear analysis in

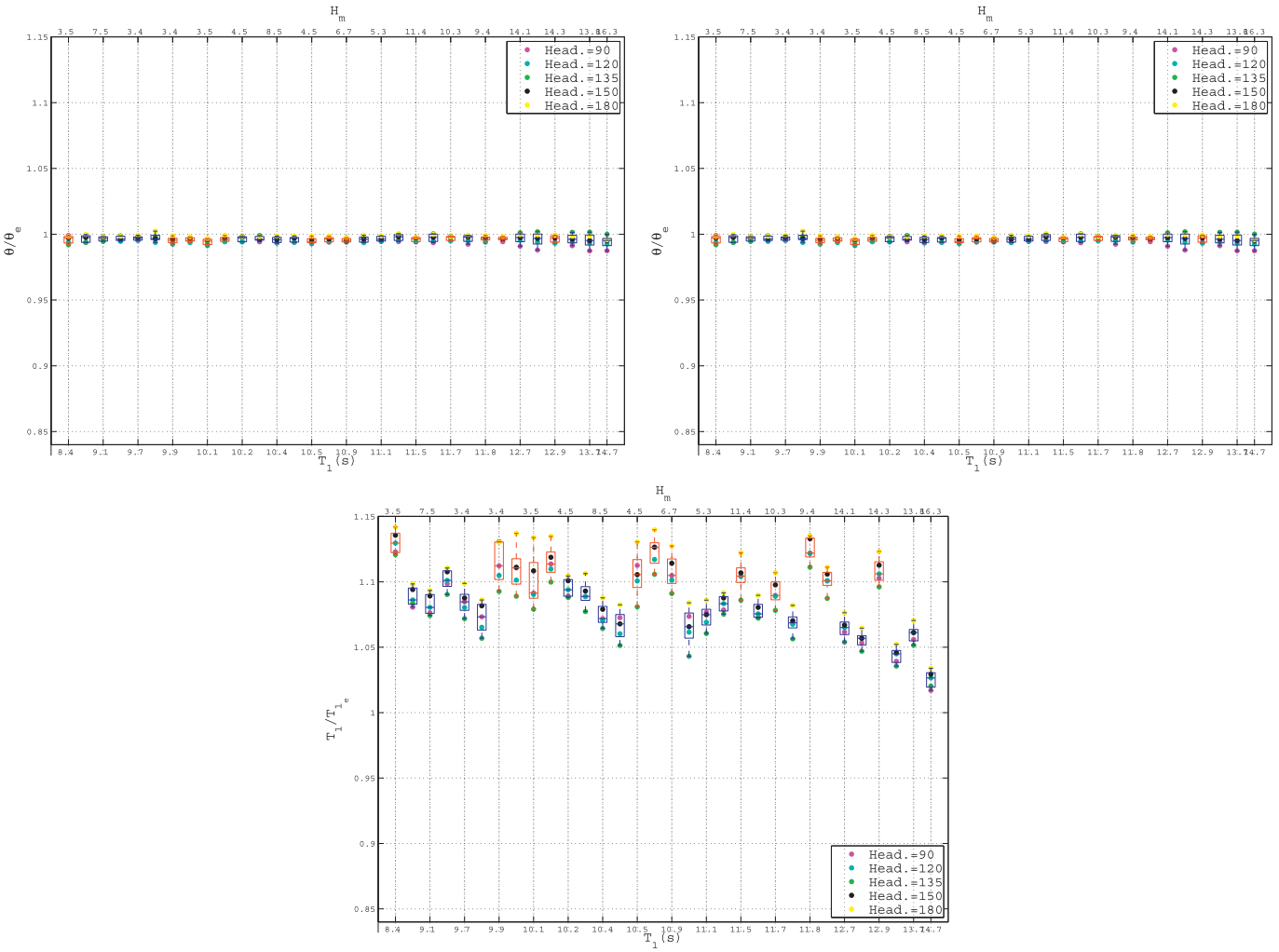


**Fig. 19.** Box plot showing the ratios between the estimated (using the variable damping RAOs) Direction, Significant wave height and Central period and the corresponding value measured using the waves probes. On each box, the central mark represents the median, the edges of the box are the 5th and 95th percentiles, finally the whiskers extend to the most extreme values obtained in each case.

**Table 4**
Mean of the relative errors obtained for $H_s$, $T_1$, $T_p$ and absolute errors in wave direction. Results presented for each wave heading and combining the tests within different ranges of $T_p$.

| | $T_p$ | JONSWAP | | | | Torsethaugen | | | |
|---|---|---|---|---|---|---|---|---|---|
| | | $T_1$ (%) | $T_p$ (%) | $H_s$ (%) | $\Delta\theta(^\circ)$ | $T_1$ (%) | $T_p$ (%) | $H_s$ (%) | $\Delta\theta(^\circ)$ |
| H90 | 9,50-11,50 | 8,06 | 2,07 | 7,53 | 0,14 | 12,29 | 3,83 | 12,27 | 0,34 |
| | 12,50-14,50 | 7,36 | 1,96 | 5,40 | 0,21 | 11,30 | 2,95 | 6,57 | 0,18 |
| | 15,50-16,90 | 5,47 | 1,43 | 2,94 | 0,14 | 8,96 | 2,35 | 6,92 | 0,31 |
| | 18,10-19,50 | 1,70 | 2,21 | 2,99 | 0,75 | 10,44 | 3,01 | 9,30 | 0,29 |
| H120 | 9,50-11,50 | 8,05 | 2,27 | 7,08 | 0,59 | 12,96 | 3,83 | 9,95 | 0,16 |
| | 12,50-14,50 | 7,06 | 1,96 | 3,81 | 1,08 | 10,73 | 2,79 | 4,12 | 1,03 |
| | 15,50-16,90 | 5,91 | 1,43 | 3,71 | 0,98 | 8,90 | 2,35 | 6,97 | 0,85 |
| | 18,10-19,50 | 2,66 | 2,21 | 3,46 | 1,90 | 10,13 | 3,01 | 6,76 | 1,04 |
| H135 | 9,50-11,50 | 7,43 | 2,07 | 4,22 | 2,27 | 12,08 | 3,83 | 6,3 | 1,12 |
| | 12,50-14,50 | 6,44 | 1,96 | 1,89 | 0,97 | 9,63 | 2,79 | 2,4 | 1,19 |
| | 15,50-16,90 | 4,93 | 1,43 | 2,23 | 0,94 | 7,82 | 2,35 | 4,78 | 0,90 |
| | 18,10-19,50 | 2,03 | 2,21 | 2,71 | 1,06 | 8,74 | 3,01 | 5,45 | 1,08 |
| H150 | 9,50-11,50 | 8,92 | 1,87 | 7,40 | 1,31 | 13,56 | 3,83 | 10,91 | 1,44 |
| | 12,50-14,50 | 7,90 | 1,96 | 4,00 | 0,56 | 12,47 | 2,79 | 6,79 | 0,77 |
| | 15,50-16,90 | 5,90 | 1,43 | 3,83 | 0,31 | 9,77 | 2,35 | 6,55 | 0,56 |
| | 18,10-19,50 | 2,94 | 2,21 | 3,70 | 0,00 | 10,84 | 3,01 | 8,04 | 0,63 |
| H180 | 9,50-11,50 | 9,84 | 2,09 | 8,45 | 0,43 | 14,19 | 3,83 | 15,35 | 0,52 |
| | 12,50-14,50 | 8,78 | 1,96 | 5,56 | 0,67 | 13,26 | 2,79 | 7,19 | 0,59 |
| | 15,50-16,90 | 6,75 | 1,43 | 4,94 | 0,63 | 10,69 | 2,35 | 8,39 | 0,43 |
| | 18,10-19,50 | 3,40 | 2,21 | 4,92 | 0,86 | 12,73 | 3,01 | 10,33 | 0,67 |

frequency domain.

Naturally, a substantial amount of future work threads arise from the topics discussed in this paper. On the one hand, an experimental analysis of the effects the moorings and risers may have on the motions of the unit is envisaged, and the same is true regarding the action of wind and current. The impact that these effects may have on the wave frequency motions and, as a consequence, on the motion-based inference must be properly quantified. A field campaign, supported by alternative wave sensors such as buoys or wave radars, is also desirable for a proper validation of the method.

Finally, further attention should also be paid to the mathematical approach of the problem, which, in principle, could be modified in order to include the uncertainty in the prediction of the RAOs. A first step in this attempt was made by Iseki (2012), who addressed this challenge with an error matrix, $C$, composed of products of the response functions and the estimation errors, achieving a modified likelihood function by the summation of the RAO matrix ($A$) and this error matrix (i.e. $B = [A + C]\mathbf{x} + U$). However, different approaches may be proposed, based on alternative prior distributions. Investigations on this topic are currently being made.

## Acknowledgments

Authors are indebted to Statoil do Brasil Óleo e Gás Ltda. for supporting the research and for making the tests campaign possible. Authors also wish to thank Petrobras, for authorizing the use of the motion-based wave inference package in this research project, and the Brazilian National Petroleum Agency (ANP). Jordi Mas-Soler acknowledges his scholarship from CAPES, the Brazilian Federal Agency for Support and Evaluation of Graduate Education. Eduardo Aoun Tannuri and Alexandre Nicolaos Simos acknowledge the Brazilian National Council for Scientific and Technological Development (CNPq) for their respective research grants (nos. 308645/2013-8 and 306687/2014-3, respectively).

## References

Akaike, H., 1980. Likelihood and the bayes procedure. Trab. Estad. Invest. Oper. 31 (1), 143–166.
Allender, J., Audunson, T., Barstow, S., Bjerken, S., Krogstad, H., Steinbakke, P., Vartdal, L., Borgman, L., Graham, C., 1989. The wadic project: a comprehensive field evaluation of directional wave instrumentation. Ocean Eng. 16 (5), 505–536.
Bispo, I.B., Simos, A.N., Tannuri, E.A., da Cruz, J.J., et al., 2012. Motion-based wave estimation by a bayesian inference method: a procedure for pre-defining the hyperparameters. In: In the 22nd International Ocean and Polar Engineering Conference. ISOPE2012, Rhodes, Greece.
Bispo, I.B., Queiroz Filho, A.N., Tannuri, E.A., Simos, A.N., 2016. Motion-based wave inference: monitoring campaign on a turret fpso. In: In the 35th International Conference on Ocean, Offshore and Arctic Engineering. OMAE2016, Busan, Korea.
Chen, Z., Zezong, C., Yanni, J., Lingang, F., Gengfei, Z., 2013. Exploration and validation of wave-height measurement using multifrequency hf radar. J. Atmos. Ocean. Technol. 30 (9), 2189–2202.
Clauss, G., Lehmann, E., Östergaard, C., 1992. Offshore Structures. Number V. 2 in Offshore Structures. Springer, ISBN 9783540197706.
Durrant, T.H., Greenslade, D.J., Simmonds, I., 2009. Validation of jason-1 and envisat remotely sensed wave heights. J. Atmos. Ocean. Technol. 26 (1), 123–134.
Faltinsen, O., 1993. Sea Loads on Ships and Offshore Structures, vol. 1. Cambridge University Press.
Fucile, F., Ludeno, G., Serafino, F., Bulian, G., Soldovieri, F., Lugni, C., 2016. Some challenges in recovering wave features from a wave radar system. In: The 26th International Ocean and Polar Engineering Conference. ISOPE2016, Rhodes, Greece.
Gemmrich, J., Thomson, J., Rogers, W.E., Pleskachevsky, A., Lehner, S., 2016. Spatial characteristics of ocean surface waves. Ocean Dynam. 66 (8), 1025–1035.
Hua, J., Palmquist, M., 1994. Wave Estimation Through Ship Motion Measurement.
Iseki, T., 2012. An improved stochastic modeling for bayesian wave estimation. In: In the 31st International Conference on Ocean. Offshore and Arctic Engineering, pp. 455–461. OMAE2012, Rio de Janeiro, Brazil.
Iseki, T., Ohtsu, K., 2000. Bayesian estimation of directional wave spectra based on ship motions. Contr. Eng. Pract. 8 (2), 215–219.
ITTC, 2014. Seakeeping experiments. In: ITTC Recommended Procedures and Guidelines. Seakeeping Committee of the 27th ITTC.
Mackay, E.B.L., 2009. Wave Energy Resource Assessment. Ph.D. Thesis. University of Southampton.
Magnusson, A.K., 2008. Forecasting extreme waves in practice. In: Olagnon, M., Prevosto, M. (Eds.), Proceedings of the Rogue Waves 2008 Workshop, pp. 1–15. Brest, France, Oct.
Mathiesen, M., Nygaard, E., 2013. Asgard Field Metocean Design Basis. Metocean Main Report (Personal communication). STATOIL.
Montazeri, N., Nielsen, U.D., 2014. Parametric estimation in the wave buoy analogy: an elaborated approach based on energy considerations. In: In the 33rd International Conference on Ocean, Offshore and Arctic Engineering. OMAE2014, San Francisco, California, USA.
Montazeri, N., Nielsen, U.D., Jensen, J.J., 2015. Trend modelling of wave parameters and application in onboard prediction of ship responses. In: OCEANS 2015-MTS/IEEE Washington. IEEE, pp. 1–8.
Montazeri, N., Nielsen, U.D., Jensen, J.J., 2016. Estimation of wind sea and swell using shipboard measurements–a refined parametric modelling approach. Appl. Ocean Res. 54, 73–86.
Morison, J., Johnson, J., Schaaf, S., et al., 1950. The force exerted by surface waves on piles. J. Petrol. Technol. 2 (05), 149–154.
Nielsen, U.D., Stredulinsky, D.C., 2012. Sea state estimation from an advancing ship a comparative study using sea trial data. Appl. Ocean Res. 34 (1), 33–44.
Nielsen, U.D., 2006. Estimations of on-site directional wave spectra from measured ship responses. Mar. Struct. 19 (1), 33–69.
Nielsen, U.D., 2007. Response-based estimation of sea state parametersinfluence of filtering. Ocean Eng. 34 (13), 1797–1810.
Nielsen, U.D., 2008. Introducing two hyperparameters in bayesian estimation of wave spectra. Probabilist. Eng. Mech. 23 (1), 84–94.
Nielsen, U.D., Galeazzi, R., Brodtkorb, A.H., 2016. Evaluation of shipboard wave estimation techniques through model-scale experiments. In: Proceedings of Oceans' 16.
Nwogu, O., 1989. Maximum entropy estimation of directional wave spectra from an array of wave probes. Appl. Ocean Res. 11 (4), 176–182.
Simos, A.N., Tannuri, E.A., Sparano, J.V., Matos, V.L., 2010. Estimating wave spectra from the motions of moored vessels: experimental validation. Appl. Ocean Res. 32 (2), 191–208.
Simos, A.N., Tannuri, E.A., da Cruz, J.J., Queiroz Filho, A.N., da Silva Bispo, I.B., Carvalho, R.C., 2012. Development of an on-board wave estimation system based on the motions of a moored fpso: commissioning and preliminary validation. In: In the 31st International Conference on Ocean. Offshore and Arctic Engineering, pp. 259–270. OMAE2012,Rio de Janeiro, Brazil.
Soares, C., Fricke, W., 2011. Advances in Marine Structures. A Balkema book. CRC Press, ISBN 9780415677714.
Stansberg, C.T., et al., 1998. On the fourier series decomposition of directional wave spectra. In: The 8th International Offshore and Polar Engineering Conference. ISOPE1998, Montral, Quebec, Canada.
Statoil, 2014. Åsgard: Statoil-operated fields in Norway. URL. http://www.statoil.com/en/ouroperations/explorationprod/ncs/aasgard/Pages/default.aspx. Accessed 19 December 2016.
Tannuri, E.A., Sparano, J.V., Simos, A.N., Da Cruz, J.J., 2003. Estimating directional wave spectrum based on stationary ship motion measurements. Appl. Ocean Res. 25 (5), 243–261.
Tannuri, E.A., Mello, P.C., Sales, J.S.J., Simos, A.N., Matos, V., 2007. Estimation of directional wave spectrum using a wave-probe array. In: Proc. Of 3rd Int. Workshop on Applied Offshore Hydrodynamics. Universidade Federal Do Rio de Janeiro.
Torsethaugen, K., Haver, S., et al., 2004. Simplified double peak spectral model for ocean waves. In: The 14th International Offshore and Polar Engineering Conference. ISOPE2004, Toulon, France.
Wijaya, T., 2009. Can a Semisubmersible Be Used as a Wave Sensor? MSc diss Norwegian University of Science and Technology(NTNU). Department of Marine Technology.